Modelling of iron-filled magneto-active polymers with a dispersed chain-like microstructure

Prashant Saxena[a,b], Jean-Paul Pelteret[a], Paul Steinmann[a]

[a]Chair of Applied Mechanics, University of Erlangen–Nuremberg,
Paul-Gordan Straße 3, Erlangen 91052, Germany
[b]Center for Integrative Genomics, University of Lausanne,
Génopode Building, 1015 Lausanne, Switzerland

Abstract

Magneto-active polymers are a class of smart materials commonly manufactured by mixing micron-sized iron particles in a rubber-like matrix. When cured in the presence of an externally applied magnetic field, the iron particles arrange themselves into chain-like structures that lend an overall anisotropy to the material. It has been observed through electron micrographs and X-ray tomographs that these chains are not always perfect in structure, and may have dispersion due to the conditions present during manufacturing or some undesirable material properties. We model the response of these materials to coupled magneto-mechanical loading in this paper using a probability based structure tensor that accounts for this imperfect anisotropy. The response of the matrix material is decoupled from the chain phase, though still being connected through kinematic constraints. The latter is based on the definition of a 'chain deformation gradient' and a 'chain magnetic field'. We conclude with numerical examples that demonstrate the effect of chain dispersion on the response of the material to magnetoelastic loading.

Keywords: Nonlinear magnetoelasticity; anisotropy; chain dispersion; finite element method

1 Introduction

Magneto-active polymers (MAPs) are smart materials in which the mechanical and the magnetic properties are coupled with each other. Typically these elastomers are composed of a rubber matrix filled with magnetisable iron particles. The magnetisable particles are usually between 1-5 μm in diameter and kept between 0-30% by volume of the entire mixture [4, 27, 36, 39]. The application of an external magnetic field causes the magnetisation of iron particles and the resulting particle-particle and particle-matrix interactions

Corresponding author: Paul Steinmann
Email: paul.steinmann@ltm.uni-erlangen.de
Ph: +49 9131 8528501, Fax: +49 9131 8528503

lead to phenomena such as magnetostriction and a change in the overall material stiffness [16, 66]. These elastomers have received considerable attention in recent times due to their potential uses in a variety of engineering applications, such as variable stiffness actuators [6] and vibration suppression by energy absorption [39, 70].

Mathematical modelling of the coupling of electromagnetic fields in deformable continua has been an area of active research in the past. In particular, we note the contributions of Landau and Lifshitz [42], Livens [43], Tiersten [64], Brown [9], Pao and Hutter [51], Maugin and Eringen [48], Maugin [46], and Eringen and Maugin [22]. The advancement of MAP (along with electro-active polymer) fabrication in the laboratory setting, and hence their wider availability in recent decades, has led to another surge in research in this area. Furthermore, as opposed to metallic alloys and ceramics, newly developed polymer based materials can undergo very large deformations. This has resulted in focused explorations in the nonlinear regime of their response.

Recent developments in this field, based on the classical works mentioned above, are largely due to Brigadnov and Dorfmann [8], Dorfmann and Ogden [19, 21], and Kankanala and Triantafyllidis [37]. The former's (Dorfmann and coworkers) work is based on the definition of a 'total' energy density function that implicitly accounts for magnetic and coupled energy stored in the polymer; while the latter's approach is to minimise a generalised potential energy with respect to internal variables, thereby yielding the relevant governing equations and boundary conditions. It is shown that any one of the magnetic induction, magnetic field, or magnetisation vectors can be used as an independent input variable and the other two obtained through constitutive relations. Based on these formulations, several nonlinear deformation problems have been studied by, for example, Dorfmann and Ogden [20], Otténio et al. [50], Bustamante et al. [13], and Danas et al. [16]. Steigmann [62] and Maugin [47] have discussed several important issues concerning the modelling of coupled magneto-electro-elasticity using continuum approaches. Further newer developments pertain to using implicit theories [12] and rate-dependent theories [55, 56] for modelling more general effects, but are beyond the scope of this work.

MAPs can exhibit isotropic or anisotropic properties depending on the kind of fabrication process used. If the elastomers are cured in the presence of an external magnetic field, the magnetisable particles tend to form chain-like arrangements lending an overall directional anisotropy to the material. Experiments on such materials [66] have shown that anisotropic MAPs tend to have stronger coupling with the external magnetic field and are therefore more likely to be used in engineering applications.

The modelling of soft elastomers with a directional anisotropy is a subject of research in its own right. For example, averaging approaches have been adopted by Galipeau and Ponte Castãneda [24] and Yin et al. [71] to capture the microscopic behaviour of aligned magnetisable particles in soft carrier. In contrast, Rudykh and Bertoldi [52] directly represented the chain-type microstructure using a laminate structure. Another common method of incorporating anisotropy, and that adopted within this work, is by using structural tensors. As described by Spencer [61] and Zheng [72], these can be coupled with the right Cauchy–Green deformation tensor to obtain scalar invariants through symmetry arguments. The invariants are then used as an independent input in the energy density function defining the material properties. This method has been used by, among others, Shams et al. [58] for modelling pre-stressed elastic solids, Holzapfel and

Gasser [31] for modelling fibre-reinforced composites, and Bustamante [10] and Danas et al. [16] for modelling MAPs with a directional anisotropy. One needs to choose at least a minimum number of invariants for completeness [18] and take care while performing energy decomposition for numerical implementation of incompressible materials [54]. Another approach towards this problem is by decoupling the response of the matrix and the anisotropic part, thereby considering different kinematic variables and energies for each. This has been used by Klinkel et al. [40] in the case of anisotropic elasto-plasticity and by Nedjar [49] for modelling anisotropic visco-elasticity. Based on this latter approach, Saxena et al. [56] recently presented a model for nonlinear magneto-viscoelasticity of anisotropic MAPs.

Recent experiments have shown another rather important feature in the microstructure of anisotropic iron-filled MAPs, namely that the particle chains formed due to the curing of an MAP under an external magnetic field are not all aligned in the same direction. The chains combined together have an average alignment in the direction of the magnetic field applied during curing, but individual chains do have an observable dispersion that may possibly influence the macroscopic response of the material. Modelling of this phenomenon and demonstration of the effect of chain dispersion on the overall macroscopic response of an MAP are the main contributions of this paper. We note that, mathematically, this phenomenon is similar to the dispersion of fibres in biological tissues as is discussed in the papers by Gasser et al. [25], Holzapfel and Ogden [32] on the modelling of blood vessels, and Federico and Herzog [23] on articular cartilage. In these works, the authors considered a generalised structure tensor based on a probability density function that accounts for the dispersion of embedded fibres.

Numerical methods, and in particular finite element analysis, have been widely used in the study of magneto-sensitive materials in order to understand and predict both their micro- and macroscopic behaviour. The formation of particle chains in magneto-rheological fluids, effectively characterising the pre-cured state of an MAP, has been investigated by Ly et al. [44] and Simon et al. [60]. For the case of solid carriers, Boczkowska et al. [5], Chen et al. [15] and Vogel et al. [68] have studied the movement of magnetic particles in elastomers. A coupled scalar magnetic potential formulation has been utilised to predict both the magnetic and deformation fields at the macroscopic level, where consideration of the surrounding free space is necessary. For example, Kannan and Dasgupta [38] adopted this approach to study the magnetostrictive behaviour of MAPs and their application in mini-actuators, Zheng and Wang [73] investigated the magnetisation of a ferromagnetic plate and Bermúdez et al. [3] demonstrated its application to electromagnets. Furthermore, the shear behaviour of a magnetised block in free space has been considered by Marvalova [45] and Bustamante et al. [13], the latter of which also investigated its contractile behaviour.

The remainder of this paper is arranged in the following manner: In section 2 we outline the fundamental aspects of continuum mechanics pertaining to magnetoelasticity. Following this, in section 3 we provide a motivation and the mathematical formulation of the dispersed magnetisable particle chains that comprise the MAP microstructure. We then detail a decoupled energy model for quasi-incompressible media in section 4, and the associated energy model for the free space. In section 5, we briefly present the finite element formulation used for performing the numerical computations. Analytical and finite element examples, used to demonstrate the behaviour captured by the constitutive

model, are presented in sections 6 and 7 respectively. Lastly, some concluding remarks are presented in section 8.

2 Kinematics, balance laws and boundary conditions

We consider a body composed of a quasi-incompressible magnetoelastic material which, in a state of no stress and no deformation, occupies the reference configuration $\mathcal{B}_0$ with a boundary $\partial\mathcal{B}_0$. In this state, the free space surrounding the body is denoted by $\mathcal{S}_0$ and the entire domain by $\mathcal{D}_0 = \mathcal{B}_0 \cup \mathcal{S}_0$. On a combined mechanical and magnetic static loading, the body occupies the spatial configuration $\mathcal{B}_t$ at time t with the boundary $\partial\mathcal{B}_t$. The corresponding configurations for the free space and entire domain are denoted by $\mathcal{S}_t$ and $\mathcal{D}_t = \mathcal{B}_t \cup \mathcal{S}_t$ respectively. A deformation function $\boldsymbol{\varphi}$ maps the points $\mathbf{X} \in \mathcal{D}_0$ to the points $\mathbf{x} \in \mathcal{D}_t$ by the relation $\mathbf{x} = \boldsymbol{\varphi}(\mathbf{X})$. The deformation gradient tensor is given by a two-point tensor $\mathbf{F} = \nabla_0 \boldsymbol{\varphi}$, ∇_0 being the differential operator with respect to $\mathbf{X}$. The determinant of $\mathbf{F}$ is given by $J = \det \mathbf{F}$ such that the condition $J > 0$ is always satisfied. For the case of an incompressible material, as presented in section 6, the constraint $J \equiv 1$ is enforced.

It is assumed that the material is electrically non-conducting and that there are no electric fields. Let $\boldsymbol{\sigma}$ be the symmetric total Cauchy stress tensor [19] that takes into account magnetic body forces, ρ be the mass density, $\mathbf{f}_m$ be the mechanical body force per unit deformed volume, $\mathbf{a}$ be the acceleration, $\mathbb{b}$ be the magnetic induction vector in $\mathcal{D}_t$, and $\mathbb{h}$ be the magnetic field vector in $\mathcal{D}_t$. The balance laws are expressed as [9, 48]

$$\nabla \cdot \boldsymbol{\sigma} + \mathbf{f}_m = \rho \mathbf{a}, \quad \boldsymbol{\sigma}^t = \boldsymbol{\sigma} \quad \text{in } \mathcal{B}_t; \quad \nabla \times \mathbb{h} = \mathbf{0}, \quad \nabla \cdot \mathbb{b} = 0 \quad \text{in } \mathcal{D}_t. \tag{1}$$

Here ∇ denotes the differential operator with respect to $\mathbf{x}$ in $\mathcal{D}_t$. Equation $(1)_1$ is the statement of balance of linear momentum, equation $(1)_2$ is the statement of balance of angular momentum, equation $(1)_3$ is a specialisation of the Ampère's law, and equation $(1)_4$ is the statement of impossibility of the existence of magnetic monopoles. The magnetic vectors are connected through the standard constitutive relation [48]

$$\mathbb{b} = \mu_0[\mathbb{h} + \mathbb{m}], \tag{2}$$

where $\mathbb{m}$ is the magnetisation vector in $\mathcal{B}_t$ (and vanishes in $\mathcal{S}_t$) and μ_0 is the magnetic permeability of vacuum. If $\boldsymbol{\sigma}_{\text{mech}}$ is the purely mechanical stress tensor, then it is related to the total stress $\boldsymbol{\sigma}$ by the relation

$$\boldsymbol{\sigma} = \boldsymbol{\sigma}_{\text{mech}} + \frac{1}{\mu_0}\left[\mathbb{b} \otimes \mathbb{b} - \frac{1}{2}[\mathbb{b} \cdot \mathbb{b}]\boldsymbol{i}\right] + [\mathbb{m} \cdot \mathbb{b}]\boldsymbol{i} - \mathbb{b} \otimes \mathbb{m}. \tag{3}$$

Here $\boldsymbol{i}$ is the second order identity tensor in $\mathcal{D}_t$ and use has been made of expression for the magnetic body force as $\mathbb{f} = [\nabla \mathbb{b}]^t \cdot \mathbb{m}$ [22, and included references].

The total (second) Piola–Kirchhoff stress and the Lagrangian forms of $\mathbb{h}, \mathbb{b}$, and $\mathbb{m}$ are defined by using the pullback operations [21, 46]

$$\mathbf{S} = J\mathbf{F}^{-1} \cdot \boldsymbol{\sigma} \cdot \mathbf{F}^{-t}, \quad \mathbb{H} = \mathbf{F}^t \cdot \mathbb{h}, \quad \mathbb{B} = J\mathbf{F}^{-1} \cdot \mathbb{b}, \quad \mathbb{M} = \mathbf{F}^t \cdot \mathbb{m}. \tag{4}$$

The above relations are used to rewrite the balance laws as

$$\nabla_0 \cdot \left(\mathbf{S} \cdot \mathbf{F}^t\right) + \rho \mathbf{f}_m = \rho \mathbf{a}, \quad \mathbf{S}^t = \mathbf{S} \quad \text{in } \mathcal{B}_0; \quad \nabla_0 \times \mathbb{H} = \mathbf{0}, \quad \nabla_0 \cdot \mathbb{B} = 0 \quad \text{in } \mathcal{D}_0, \tag{5}$$

along with the relation for magnetic quantities

$$J^{-1}\mathbf{C} \cdot \mathbb{B} = \mu_0 \left[\mathbb{H} + \mathbb{M}\right]. \tag{6}$$

At a boundary $\partial\mathcal{B}_t$, which can be the bounding surface of the magnetoelastic body or a surface of discontinuity within the material, the jump conditions

$$\mathbf{n} \times [\![\mathbb{h}]\!] = \mathbf{0}, \quad \mathbf{n} \cdot [\![\mathbb{b}]\!] = 0, \tag{7}$$

need to be satisfied by the magnetic vectors. Here $\mathbf{n}$ denotes the unit outward normal to $\partial\mathcal{B}_t$, and $[\![\bullet]\!] = [\bullet]^{\text{out}} - [\bullet]^{\text{in}}$ represents jump in a quantity across the boundary. The total Cauchy stress must satisfy

$$\boldsymbol{\sigma} \cdot \mathbf{n} = \mathbf{t}_a + \mathbf{t}_m, \tag{8}$$

where $\mathbf{t}_a$ and $\mathbf{t}_m$ are, respectively, the mechanical and magnetic contributions to the traction per unit area on $\partial\mathcal{B}_t$. In the reference configuration, the boundary conditions at the boundary $\partial\mathcal{B}_0$ are given by

$$\mathbf{N} \times [\![\mathbb{H}]\!] = \mathbf{0}, \quad \mathbf{N} \cdot [\![\mathbb{B}]\!] = 0, \quad \mathbf{F} \cdot \mathbf{S} \cdot \mathbf{N} = \mathbf{t}_A + \mathbf{t}_M, \tag{9}$$

where $\mathbf{N}$ is the unit outward normal to $\partial\mathcal{B}_0$ and related to $\mathbf{n}$ through Nanson's formula $\mathbf{n}\,\mathrm{d}a = J\mathbf{F}^{-t} \cdot \mathbf{N}\,\mathrm{d}A$, where $\mathrm{d}a$ and $\mathrm{d}A$ represent the infinitesimal current and reference areas, respectively. The vectors $\mathbf{t}_A$ and $\mathbf{t}_M$ are the mechanical and magnetic contributions to the traction per unit area on $\partial\mathcal{B}_0$.

3 Magneto-active polymer microstructure and chain dispersion

In order to understand the particle chain alignment and resulting anisotropy in magneto-active polymers, we analyse the electron micrographs of MAP samples documented by Jolly et al. [36] and Boczkowska and Awietjan [4]. It is observed that the MAPs cured under the effect of a magnetic field develop a preferred direction due to the alignment of iron particles in chain-like formations. Under (presumably) near ideal curing conditions, the chains are quite uni-directional as can be seen in figure 2(a) of [4]. However, if one varies the matrix material or the particle volume fraction (figures 1(c) and 2(c,d,e) of [4]), we observe that the particle chains do have an observable dispersion.

To reaffirm this observation, samples of magneto-active polymers were prepared and their microstructure subsequently analysed using X-ray computed tomography. Iron particles coated with silicon-dioxide were mixed with ELASTOSIL® and the mixture was cured for sixteen hours in the presence of a magnetic field created by permanent magnets. The volume fraction of iron particles was taken to be 2% and 10%. Dispersion of the formed particle chains is quite prevalent in the samples shown in figure 1. Overall, it is hypothesised that the final microstructure was influenced by a multitude of factors

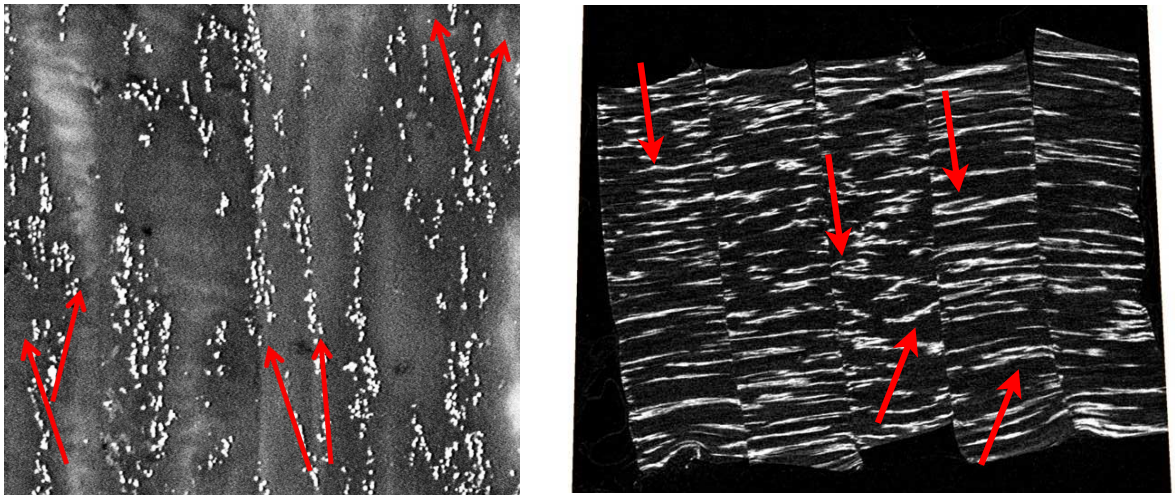

(a) (b)

Figure 1: (a) SEM image of an MAP with 10% iron particles by volume. Non-uniform local directions of alignment of the particle chains are represented by red arrows. (b) Computer Tomograph of 5 stacked samples of an MAP with 2% of iron particles by volume. The non-uniform distribution and alignment of the particle chains, examples of which are marked by red arrows, is clearly visible.

present during the curing stage of sample preparation. Examples of these influences include the gel point and viscosity of the matrix during its fluid state and the strength and the duration of the magnetic field to which the uncured material was exposed.

In all of the cases described above, the collection of chains have an effective direction along the applied magnetic induction. However, all the chains individually do not align in such a way as shown in the right example in figure 2. Rather, as is shown in the middle sketch, the particle chains may be imperfectly formed and non-uniformly aligned. This is an important aspect of the material microstructure and should be modelled appropriately.

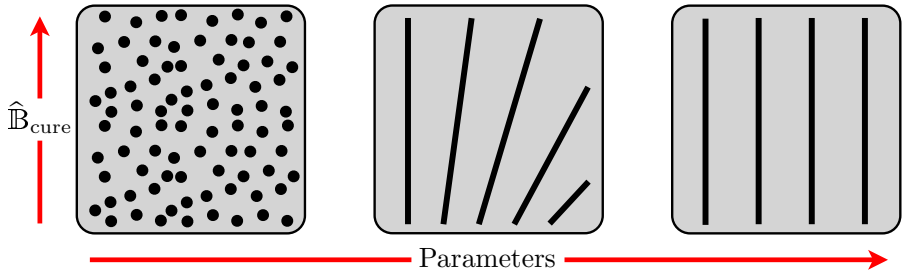

Figure 2: Depiction of the possible range of particle microstructures present in a magneto-sensitive elastomer cured under a uniform magnetic field. Depending on the curing conditions, the end-product may be isotropic (left), have perfect particle-chain formation (right) or a state between the two extremes.

Gasser et al. [25] and Holzapfel and Ogden [32] have modelled fibre dispersion in anisotropic soft matter with application to blood vessels. The fibres in biological tissues, though with an average alignment in a preferred direction, have an observable dispersion

that significantly affects their mechanical properties. A similar analysis for collagen fibre distribution in bone cartilage has been performed by Federico and Herzog [23]. In the following text, we use similar concepts to approach the problem of particle-chain distribution in magnetorheological elastomers.

A unit direction vector $\mathbf{M}$ is characterised by means of Eulerian angles $\theta \in [0, \pi]$ and $\phi \in [0, 2\pi]$ in a three-dimensional coordinate system $\{\mathbf{e}_1, \mathbf{e}_2, \mathbf{e}_3\}$ such that

$$\mathbf{M}(\theta, \phi) = \sin\theta\cos\phi\,\mathbf{e}_1 + \sin\theta\sin\phi\,\mathbf{e}_2 + \cos\theta\,\mathbf{e}_3. \tag{10}$$

If the unit vector $\mathbf{M}(\theta, \phi)$ represents the direction of a particle chain, then the overall generalised structure tensor $\mathbf{G}$ for the material can be defined as

$$\mathbf{G} = \frac{1}{4\pi}\int_{\omega} \xi(\mathbf{M}(\theta,\phi))\,\mathbf{M}(\theta,\phi)\otimes\mathbf{M}(\theta,\phi)\,d\omega, \tag{11}$$

where ω is the unit sphere, $d\omega = \sin\theta\,d\theta\,d\phi$ and ξ is a probability density function defining orientation of the particle chains such that $\xi(\mathbf{M})$ is normalised according to the relation

$$\frac{1}{4\pi}\int_{\omega} \xi(\mathbf{M}(\theta,\phi))\,d\omega = 1. \tag{12}$$

In the ideal case of absolute anisotropy when all the particle chains are aligned along just one direction (say $\mathbf{M} = \mathbf{e}_3$), then the probability density function ξ approaches the limit of a Dirac-Delta and the structure tensor $\mathbf{G}$ reduces to

$$\mathbf{G} = \mathbf{M}\otimes\mathbf{M}. \tag{13}$$

For true material characterisation, the probability density function ξ can be numerically approximated using experimental data obtained through three-dimensional computerised-tomography (CT) scans of the material specimens. For some simple cases, it can also be approximated through two-dimensional electron-microscopy (SEM or TEM) images. In this paper, for the sake of simplicity, we employ symmetry arguments and assume a transversally isotropic distribution of particle chains around an axis such that the probability ξ simply depends on the angle θ with no dependence on ϕ. Following [25] we assume the function ξ to be given by the π-periodic von Mises probability distribution function

$$\xi(\theta) = 4\sqrt{\frac{b}{2\pi}}\frac{\exp\left(b\left[\cos 2\theta + 1\right]\right)}{\operatorname{erfi}\left(\sqrt{2b}\right)}. \tag{14}$$

where the parameter $b \in [0, \infty]$. This causes the structure tensor $\mathbf{G}$ to reduce to the following simple form

$$\mathbf{G} = \kappa\mathbf{I} + [1 - 3\kappa]\overline{\mathbf{M}}\otimes\overline{\mathbf{M}} \tag{15}$$

as has been shown by Gasser et al. [25]. Here $\overline{\mathbf{M}}$ is the direction of average chain alignment and $\kappa \in [0, 1/3]$ is a parameter given by

$$\kappa = \frac{1}{4}\int_{0}^{\pi} \xi(\theta)\sin^3\theta\,d\theta, \tag{16}$$

and describes the 'degree of anisotropy' of the material. The parameters κ and b have a one-to-one mapping through the relations (14) and (16). A visual interpretation of the presented dispersed microstructure model and its parameters, specifically in the context of a magneto-sensitive material, is provided in figure 3. Figure 4 presents 3-D plots of the von Mises probability distribution as given in equation (14) for different values of the dispersion parameter κ.

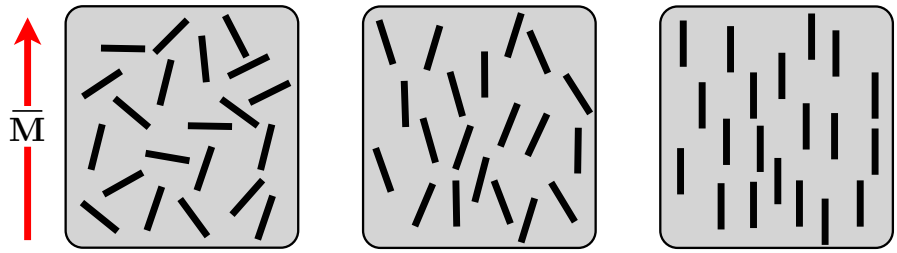

$\kappa = \frac{1}{3}$ $\kappa = 0.05$ $\kappa = 0$

Figure 3: Description of material structure assumed by the material model. For a given average chain direction $\overline{\mathbf{M}}$, the upper and lower limiting values for κ respectively represent an isotropic and perfectly transversely isotropic material. For the isotropic case, this may imply that either the particles do not form chain-like structures, or the particle chains are completely randomly orientated. An intermediate value of κ assumes that partial organisation of particle chains towards $\overline{\mathbf{M}}$ has taken place during curing.

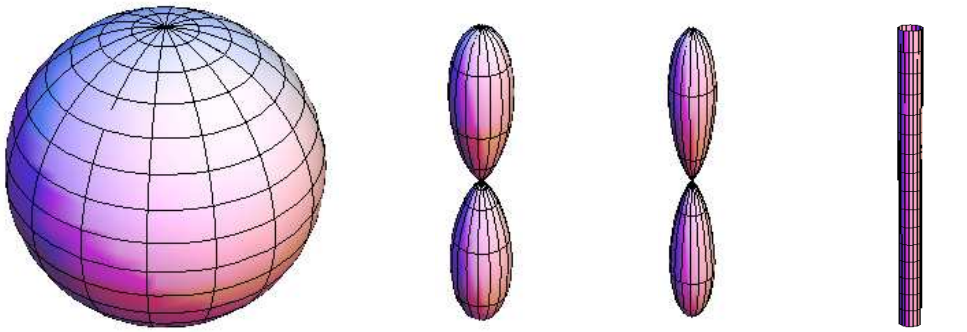

$\kappa = 1/3$ $\kappa = 0.1$ $\kappa = 0.05$ $\kappa = 0$

Figure 4: Probability density distribution plotted on a unit sphere according to equation (14) corresponding to two extreme and two intermediate values of the dispersion parameter κ.

4 Constitutive modelling

In general, we consider the total magnetoelastic energy of the material to depend on the deformation gradient, the magnetic field vector and the structure tensor, that is

$$\Omega_0 = \Omega_0(\mathbf{F}, \mathbb{H}, \mathbf{G}). \tag{17}$$

It can be shown that, using symmetry arguments, the dependence on $\mathbf{F}$ is simplified through a dependence on the right Cauchy–Green deformation tensor $\mathbf{C} = \mathbf{F}^t \cdot \mathbf{F}$. For

this case, the total Piola–Kirchhoff stress and the magnetic induction are given by the constitutive relations [21]

$$\mathbf{S} = 2\frac{\partial \Omega_0}{\partial \mathbf{C}}, \qquad \mathbb{B} = -\frac{\partial \Omega_0}{\partial \mathbb{H}}. \tag{18}$$

4.1 Decoupled energy model

In order to take into account the response of the magnetoelastic chains, we follow the approach presented in a recent paper [56] that is based on the modelling of fibre-reinforced solids by Klinkel et al. [40]. We define a chain-deformation gradient $\mathbf{F}^c$ such that

$$\mathbf{F}^c = \mathbf{F} \cdot \mathbf{G} = \kappa \mathbf{F} + [1 - 3\kappa]\mathbf{F} \cdot \mathbf{A}. \tag{19}$$

where we have defined $\mathbf{A} = \overline{\mathbf{M}} \otimes \overline{\mathbf{M}}$. Indeed, we note that if one defines the chain deformation gradient as an average over chains in all the directions

$$\mathbf{F}^c = \frac{1}{4\pi} \int\limits_{\omega} \xi \left[\mathbf{F} \cdot \mathbf{M}\right] \otimes \mathbf{M} \, d\omega, \tag{20}$$

we arrive at the expression in (19) on using the condition (11). In the limit $\kappa \to 0$ for a purely anisotropic material with no dispersion, this reduces to $\mathbf{F}^c = \mathbf{F} \cdot \mathbf{A}$ thus capturing the one-dimensional deformation in the chain anisotropy direction. We note that here and henceforth, a superscript 'c' refers to the quantities associated with the chain phase.

For future use, we define $\mathbf{C}^c = [\mathbf{F}^c]^t \cdot \mathbf{F}^c$, also expressed as

$$\mathbf{C}^c = \mathbf{G} \cdot \mathbf{C} \cdot \mathbf{G} = \kappa^2 \mathbf{C} + \kappa[1 - 3\kappa][\mathbf{C} \cdot \mathbf{A} + \mathbf{A} \cdot \mathbf{C}] + [1 - 3\kappa]^2 [\mathbf{C} : \mathbf{A}]\mathbf{A}, \tag{21}$$

and present the identity

$$\frac{\partial \mathbf{C}^c}{\partial \mathbf{C}} = \mathbf{G} \overline{\otimes} \mathbf{G} = \kappa^2 \mathbb{I}_4 + \frac{\kappa}{2}[1 - 3\kappa]\left[\mathbf{I} \overline{\otimes} \mathbf{A} + \mathbf{I} \underline{\otimes} \mathbf{A} + \mathbf{A} \underline{\otimes} \mathbf{I} + \mathbf{I} \overline{\otimes} \mathbf{A}\right] + [1 - 3\kappa]^2 \mathbf{A} \otimes \mathbf{A}. \tag{22}$$

Here we define the non-standard tensor products of two second order tensors as $[\mathbf{P} \overline{\otimes} \mathbf{Q}]_{ijkl} = P_{ik}Q_{jl}$ and $[\mathbf{P} \underline{\otimes} \mathbf{Q}]_{ijkl} = P_{il}Q_{jk}$, and $\mathbb{I}_4 = \left[\mathbf{I} \overline{\otimes} \mathbf{I} + \mathbf{I} \underline{\otimes} \mathbf{I}\right]/2$ is the fourth order symmetric identity tensor.

The Lagrangian magnetic field in the average chain direction is given by

$$\mathbb{H}^c = \mathbf{G} \cdot \mathbb{H} = \kappa \mathbb{H} + [1 - 3\kappa][\overline{\mathbf{M}} \cdot \mathbb{H}]\overline{\mathbf{M}}, \tag{23}$$

and we note the identity

$$\frac{\partial \mathbb{H}^c}{\partial \mathbb{H}} = \mathbf{G}. \tag{24}$$

The dependence of the total energy density on the structure tensor $\mathbf{G}$ is now considered implicitly through $\mathbf{C}^c$ and $\mathbb{H}^c$. Thus $\Omega_0 = \Omega_0(\mathbf{C}, \mathbf{C}^c, \mathbb{H}, \mathbb{H}^c)$ and the Piola–Kirchhoff stress is given in the case of incompressibility by

$$\mathbf{S} = 2\frac{\partial \Omega_0}{\partial \mathbf{C}} + 2\kappa^2 \frac{\partial \Omega_0}{\partial \mathbf{C}^c} + 2\kappa[1 - 3\kappa]\left[\mathbf{A} \cdot \frac{\partial \Omega_0}{\partial \mathbf{C}^c} + \frac{\partial \Omega_0}{\partial \mathbf{C}^c} \cdot \mathbf{A}\right] + 2[1 - 3\kappa]^2 \left[\frac{\partial \Omega_0}{\partial \mathbf{C}^c} : \mathbf{A}\right] \mathbf{A} - p\mathbf{C}^{-1}, \tag{25}$$

while the magnetic induction is given as

$$\mathbb{B} = -\frac{\partial \Omega_0}{\partial \mathbb{H}} - \mathbf{G} \cdot \frac{\partial \Omega_0}{\partial \mathbb{H}^c}. \tag{26}$$

4.2 Dealing with material incompressibility

The energy density function is initially decomposed into two parts, namely those attributed to the matrix and the particle chain, such that

$$\Omega_0 = \Omega_0^{\text{mat}}(\mathbf{C}, \mathbb{H}) + \Omega_0^c(\mathbf{C}, \mathbf{C}^c, \mathbb{H}, \mathbb{H}^c). \tag{27}$$

However, following the discussion by Sansour [54], only the matrix part is decomposed further into volumetric and isochoric parts [59] such that

$$\Omega_0 = \underbrace{\Omega_0^{\text{vol}}(J) + \widetilde{\Omega}_0^{\text{iso}}(\widetilde{\mathbf{C}}, \mathbb{H})}_{\Omega_0^{\text{mat}}} + \Omega_0^c(\mathbf{C}, \mathbf{C}^c, \mathbb{H}, \mathbb{H}^c). \tag{28}$$

A multiplicative split of the deformation gradient into volumetric and isochoric contributions

$$\mathbf{F} = \widehat{\mathbf{F}} \cdot \widetilde{\mathbf{F}} \quad \text{with} \quad \widehat{\mathbf{F}} := J^{\frac{1}{3}}\mathbf{I}, \quad \widetilde{\mathbf{F}} := J^{-\frac{1}{3}}\mathbf{F} \tag{29}$$

is also assumed [59], from which the isochoric part of the right Cauchy–Green deformation tensor is given as $\widetilde{\mathbf{C}} = \widetilde{\mathbf{F}}^t \cdot \widetilde{\mathbf{F}}$. Such decompositions are typically utilised not only to capture the decoupled behaviour of rubber-like materials but also to support their numerical modelling. In view of the material description given by equation (28), for the case of a quasi-incompressible material equation $(18)_1$ is transformed to

$$\mathbf{S} = 2\left[\frac{\partial \widetilde{\Omega}_0^{\text{iso}}}{\partial \widetilde{\mathbf{C}}} : \frac{\partial \widetilde{\mathbf{C}}}{\partial \mathbf{C}} + \frac{\partial \Omega_0^c}{\partial \mathbf{C}}\right] - pJ\mathbf{C}^{-1} \tag{30}$$

with the hydrostatic pressure defined as

$$p = -\frac{\partial \Omega_0^{\text{vol}}(J)}{\partial J}. \tag{31}$$

4.3 Dealing with surrounding free space

In addition to the stored energy in the material due to elastic deformation and magnetisation, an additional energy contribution arises due to the presence of the magnetic field permeating and surrounding the elastic body. Depending on its constitutive model and consequent magnetisation, this may be a negligible quantity inside the elastic body. However, this energy must certainly be accounted for in the free space as it quantifies its Maxwell stress and free space induction. We therefore formally write the total stored potential energy Ω_0 as

$$\Omega_0(\mathbf{C}, \mathbb{H}) = W_0(\mathbf{C}, \mathbb{H}) + M_0(\mathbf{C}, \mathbb{H}) \tag{32}$$

where W_0 is the elastic and magnetic energy stored in the elastic body and $M_0 = -\frac{1}{2}\mu_0 J\mathbf{C}^{-1} : \mathbb{H} \otimes \mathbb{H}$ is the energy stored in the free space [67]. It should be noted that, for the examples shown later, the free space energy within the elastic media is ignored and the above reduces to

$$\Omega_0(\mathbf{C}, \mathbb{H}) \equiv W_0(\mathbf{C}, \mathbb{H}) \text{ if } \mathbf{X} \in \mathcal{B}_0 \quad \text{and} \quad \Omega_0(\mathbf{C}, \mathbb{H}) \equiv M_0(\mathbf{C}, \mathbb{H}) \text{ if } \mathbf{X} \in \mathcal{S}_0. \tag{33}$$

5 Finite element formulation

Under the assumption of quasi-static conditions and the presence of no free-currents, we denote the displacement by $\mathbf{u} = \mathbf{x} - \mathbf{X}$ and define a scalar magnetic potential[1] Φ [7, 41]. The referential magnetic field, being curl-free, is related to the magnetic potential (a fictitious quantity) by

$$\mathbb{H} = -\nabla_0 \Phi \tag{34}$$

with the following conditions on the solid boundary and truncated far-field boundary $\partial\mathcal{S}_\infty$

$$[\![\Phi]\!] = 0 \quad \text{on} \quad \partial\mathcal{B}_0, \quad \Phi = \overline{\Phi} \quad \text{on} \quad \partial\mathcal{S}_\infty. \tag{35}$$

We define a total potential energy functional

$$\Pi = \Pi^{\text{int}} + \Pi^{\text{ext}} \tag{36}$$

on the domain $\mathcal{D}_0$, composed of a magnetoelastic subdomain $\mathcal{B}_0$ and the surrounding free space $\mathcal{S}_0$. The total internal potential energy is given by

$$\Pi^{\text{int}} = \int_{\mathcal{D}_0} \Omega_0 \left(\mathbf{C}, \mathbb{H}\right) = \int_{\mathcal{B}_0} W_0 \left(\mathbf{C}, \mathbf{C}^c, \mathbb{H}, \mathbb{H}^c\right) + \int_{\mathcal{S}_0} M_0 \left(\mathbf{C}, \mathbb{H}\right), \tag{37}$$

where, from equations (28) and (32), W_0 denotes the total potential energy per unit volume due to the magnetoelastic material's deformation and magnetisation, while M_0 quantifies the magnetic energy stored in the free field. The total external potential energy is

$$\Pi^{\text{ext}} = -\int_{\mathcal{B}_0} \mathbf{u} \cdot \mathbf{b}_0 - \int_{\Gamma_0^t} \mathbf{u} \cdot \mathbf{t}_A - \int_{\partial\mathcal{S}_\infty^b} \Phi \left[\mathbf{B}_A \cdot \mathbf{N}_\infty\right], \tag{38}$$

where $\mathbf{b}_0, \mathbf{t}_A$ represent the referential mechanical body forces and surface tractions respectively, and $\mathbf{B}_A$ is the magnetic induction prescribed on the far-field boundary $\partial\mathcal{S}_\infty^b$.

Using the principle of stationary potential energy, the equilibrium solution to equation (36) can be determined. The stationary point is that at which all directional derivatives of the total potential energy disappear. The expression for the Gâteaux derivative of the total energy is

$$\begin{aligned} \delta\Pi\left(\mathbf{u}, \delta\mathbf{u}, \Phi, \delta\Phi\right) &= \delta_{\mathbf{u}}\Pi\left(\mathbf{u}, \Phi\right) + \delta_{\Phi}\Pi\left(\mathbf{u}, \Phi\right) \\ &= \frac{d}{d\epsilon}\Pi\left(\mathbf{u} + \epsilon\delta\mathbf{u}, \Phi\right)\Big|_{\epsilon=0} + \frac{d}{d\gamma}\Pi\left(\mathbf{u}, \Phi + \gamma\delta\Phi\right)\Big|_{\gamma=0} = 0, \end{aligned} \tag{39}$$

[1] An alternative to the scalar potential formulation, which is used due to its simple numerical implantation, is the vector potential formulation [11, 41, 57] for which a relationship between $\mathbb{B}$ and a vector potential field $\mathbb{A}$, namely $\mathbb{B} = \nabla_0 \times \mathbb{A}$, is assumed.

which yields $\delta\Pi = \delta\Pi^{\text{int}} + \delta\Pi^{\text{ext}}$. Using equations (33) and (37), the variation of the internal potential energy is expressed concisely as

$$\delta\Pi^{\text{int}} = \delta_{\mathbf{u}}\Pi^{\text{int}} + \delta_{\Phi}\Pi^{\text{int}} = \int_{\mathcal{D}_0} \delta\mathbf{E} : \mathbf{S} - \int_{\mathcal{D}_0} \delta\mathbb{H}\cdot\mathbb{B}, \tag{40}$$

and that of the external potential energy is

$$\delta\Pi^{\text{ext}} = -\int_{\mathcal{B}_0} \delta\mathbf{u}\cdot\mathbf{b}_0 - \int_{\Gamma_0^t} \delta\mathbf{u}\cdot\mathbf{t}_A - \int_{\partial\mathcal{S}_\infty^b} \delta\Phi\,[\mathbf{B}_A\cdot\mathbf{N}_\infty]. \tag{41}$$

Here we define the variations of the Green-Lagrange strain tensor, the deformation gradient and magnetic field respectively as

$$\delta\mathbf{E} = \text{sym}\left[\mathbf{F}^T\cdot\delta\mathbf{F}\right], \quad \delta\mathbf{F} = \nabla_0\delta\mathbf{u}, \quad \delta\mathbb{H} = -\nabla_0\delta\Phi. \tag{42}$$

As is detailed by Bustamante and Ogden [11] for the case involving both a solid and free-space domain, the above collectively represents the equivalent weak form of the divergence-free condition for both the stress and magnetic induction (equations $(1)_{1,4}$) for the magneto-elastostatic case. Furthermore, the continuity of the normal traction and magnetic induction (given in equation $(7)_2$) at the material interfaces is also embedded within this formulation. However, it remains to be ensured that the compatibility conditions for the deformation and the continuity of tangential magnetic field (equation $(7)_1$) are satisfied.

As the material laws are nonlinear, an iterative procedure such as the Newton-Raphson method must be utilised to determine the stationary point. The nonlinear system of equations can be linearised using a first-order Taylor expansion about the current solution. Linearisation of equation (40) with respect to the motion and scalar magnetic potential renders the contributions [63, 69]

$$\Delta\delta\Pi^{\text{int}} = \Delta_{\mathbf{u}}\left[\delta_{\mathbf{u}}\Pi^{\text{int}} + \delta_{\Phi}\Pi^{\text{int}}\right] + \Delta_{\Phi}\left[\delta_{\mathbf{u}}\Pi^{\text{int}} + \delta_{\Phi}\Pi^{\text{int}}\right], \tag{43}$$

$$\begin{aligned} &= \int_{\mathcal{D}_0} \left[\text{sym}\left[\delta\mathbf{F}^T\cdot\Delta\mathbf{F}\right] : \mathbf{S} + \delta\mathbf{E} : \boldsymbol{\mathcal{H}} : \Delta\mathbf{E} - \delta\mathbb{H}\cdot\mathbb{P} : \Delta\mathbf{E}\right] \\ &+ \int_{\mathcal{D}_0} \left[-\delta\mathbf{E} : \mathbb{P}^T\cdot\Delta\mathbb{H} - \Delta\mathbb{H}\cdot\mathbf{D}\cdot\Delta\mathbb{H}\right], \end{aligned} \tag{44}$$

with $\Delta(\bullet)$ representing value increments. The material tangents, namely the referential elasticity tensor, the fully-referential magneto-elasticity tensor and the rank-2 magnetic tensor, are defined as

$$\begin{aligned} \boldsymbol{\mathcal{H}} &= 4\frac{\partial^2\Omega_0(\mathbf{C},\mathbb{H})}{\partial\mathbf{C}\otimes\partial\mathbf{C}}, \quad \mathbb{P} = -2\frac{\partial^2\Omega_0(\mathbf{C},\mathbb{H})}{\partial\mathbf{C}\otimes\partial\mathbb{H}}, \\ \mathbb{P}^T &= -2\frac{\partial^2\Omega_0(\mathbf{C},\mathbb{H})}{\partial\mathbb{H}\otimes\partial\mathbf{C}}, \quad \mathbf{D} = -\frac{\partial^2\Omega_0(\mathbf{C},\mathbb{H})}{\partial\mathbb{H}\otimes\partial\mathbb{H}}. \end{aligned} \tag{45}$$

Overall, the linear Taylor expansion of equation (40), with the use of equation (43), can be expressed as

$$\begin{aligned} 0 &= \delta_{\mathbf{u}}\Pi + \Delta_{\mathbf{u}}\delta_{\mathbf{u}}\Pi + \Delta_{\Phi}\delta_{\mathbf{u}}\Pi \\ 0 &= \delta_{\Phi}\Pi + \Delta_{\mathbf{u}}\delta_{\Phi}\Pi + \Delta_{\Phi}\delta_{\Phi}\Pi. \end{aligned} \tag{46}$$

5.1 Space discretisation

The displacement and scalar magnetic potential fields are spatially discretised by introducing a finite element basis

$$\mathbf{u}\left(\mathbf{X}\right) = \sum_I u^I \mathbf{N}^I\left(\mathbf{X}\right), \quad \Phi\left(\mathbf{X}\right) = \sum_I \Phi^I N^I\left(\mathbf{X}\right), \tag{47}$$

$$\nabla_0 \mathbf{u}\left(\mathbf{X}\right) = \sum_I u^I \nabla_0 \mathbf{N}^I\left(\mathbf{X}\right), \quad \nabla_0 \Phi\left(\mathbf{X}\right) = \sum_I \Phi^I \nabla_0 N^I\left(\mathbf{X}\right). \tag{48}$$

where $\mathbf{N}^I$ and N^I are, respectively, the vector-valued and scalar-valued shape functions corresponding to degree-of-freedom I. This description of the spatial discretisation allows for the discrete system to be presented in a manner that parallels its implementation in the finite element framework. Furthermore, the Galerkin finite element method is adopted such that the resulting system is square and symmetric. The variation and linearisation of the discretised fields follows as

$$\delta\mathbf{u}\left(\mathbf{X}\right) = \sum_I \delta u^I \mathbf{N}^I\left(\mathbf{X}\right), \quad \delta\Phi\left(\mathbf{X}\right) = \sum_I \delta\Phi^I N^I\left(\mathbf{X}\right), \tag{49}$$

$$\Delta\mathbf{u}\left(\mathbf{X}\right) = \sum_I \Delta u^I \mathbf{N}^I\left(\mathbf{X}\right), \quad \Delta\Phi\left(\mathbf{X}\right) = \sum_I \Delta\Phi^I N^I\left(\mathbf{X}\right). \tag{50}$$

The variations vanish on the Dirichlet boundaries; that is to say that $\delta\mathbf{u} = \mathbf{0}$ on $\partial\mathcal{B}_0^{\varphi}$ and $\delta\Phi = 0$ on $\partial\mathcal{S}_0^{\Phi}$. As the free-space by definition has no elastic degrees-of-freedom and offers no impediment to the movement of the solid media, we further impose the condition that $\delta\mathbf{u} = \mathbf{0}$ on $\mathcal{S}_0 \backslash \Gamma_0^{ds}$, where $\Gamma_0^{ds} = \mathcal{S}_0 \cap \mathcal{B}_0$ denotes the surfaces of the solid body exposed to the free-space.

Noting that the resulting equation must hold for all arbitrary variations $\delta u^I, \delta\Phi^I$, a system of linear equations can be resolved. Following from equation (46), the discrete form of the algebraic equations to be solved at time t and Newton iterate n is

$$\begin{bmatrix} \mathbf{K}_{\mathbf{uu}} & \mathbf{K}_{\mathbf{u}\Phi} \\ \mathbf{K}_{\Phi\mathbf{u}} & \mathbf{K}_{\Phi\Phi} \end{bmatrix} \begin{bmatrix} \Delta\mathbf{u} \\ \Delta\Phi \end{bmatrix} = \begin{bmatrix} \mathbf{f}_{\mathbf{u}} \\ \mathbf{f}_{\Phi} \end{bmatrix} \quad \Rightarrow \quad \mathbf{K}\cdot\Delta\mathbf{d} = \mathbf{f} = -\mathbf{r} \tag{51}$$

where $\mathbf{d} = \left[\mathbf{u} \;\; \Phi\right]^T$ collectively denotes the values of the field variables and $\mathbf{r}$ the residual vector. The corresponding solution update is given by

$$\mathbf{d}^{n+1} = \mathbf{d}^n + \Delta\mathbf{d}^n, \tag{52}$$

and contributions to the stiffness matrix and right-hand side vector from degrees-of-freedom I, J are

$$\begin{aligned} K^{IJ} = \int_{\mathcal{D}_0} \Big[& \left[\nabla_0^T \mathbf{N}^I \cdot \nabla_0 \mathbf{N}^J\right] : \mathbf{S} + \left[\mathbf{F}^T \cdot \nabla_0 \mathbf{N}^I\right] : \boldsymbol{\mathcal{H}} : \left[\mathbf{F}^T \cdot \nabla_0 \mathbf{N}^J\right] \\ & + \nabla_0 N^I \cdot \mathbb{P} : \left[\mathbf{F}^T \cdot \nabla_0 \mathbf{N}^J\right] + \left[\mathbf{F}^T \cdot \nabla_0 \mathbf{N}^I\right] : \mathbb{P}^T \cdot \nabla_0 N^J \\ & - \nabla_0 N^I \cdot \mathbf{D} \cdot \nabla_0 N^J \Big], \end{aligned} \tag{53}$$

$$f^I = \int_{\mathcal{B}_0} \mathbf{N}^I \cdot \mathbf{b}_0 + \int_{\Gamma_0^t} \mathbf{N}^I \cdot \mathbf{t}_A - \int_{\mathcal{D}_0} \Big[\left[\mathbf{F}^T \cdot \nabla_0 \mathbf{N}^I\right] : \mathbf{S} + \nabla_0 N^I \cdot \mathbb{B} \Big]. \tag{54}$$

5.2 Mesh-motion in the free-space

As the energies given in equation (37) are defined in terms of referential quantities, an expression for the displacement $\mathbf{u}$ is required for the entire computational domain. More pointedly, it is necessary that some artificial measure of deformation be provided within the free-space $\mathcal{S}_0$ such that an associated, invertible deformation gradient (which maps the configuration used for computation to the physically relevant spatial configuration) can be defined and spatial quantities derived from M_0 can be computed.

Moving mesh approaches adapted from the modelling of fluid systems with moving boundaries (the "ALE" class of fluid formulations) can be utilised in magneto-elastic problems [14, 53]. Johnson and Tezduyar [35] describes a typical approach to performing this update, and the one that is used in this work. Once the deformation field in the solid media is computed, we solve a linear elasticity problem

$$\int_{\mathcal{S}_0} \nabla\delta\mathbf{u}^* : \boldsymbol{\sigma}^* = 0 \quad \text{with} \quad \boldsymbol{\sigma}^* = \boldsymbol{\mathcal{K}}^*(\mathbf{X}) : \boldsymbol{\varepsilon}^* \quad , \quad \boldsymbol{\varepsilon}^* = \frac{1}{2}\left[\nabla\mathbf{u}^* + (\nabla\mathbf{u}^*)^T\right]. \tag{55}$$

The motion of the mesh in the free-space is thus governed by a fictitious stiffness tensor defined at each integration point and the assumed Dirichlet boundary conditions. There exist a number of viable choices to define an effective stiffness to the elasticity problem [34, 35] and we choose to point-wise define the isotropic elasticity tensor

$$\boldsymbol{\mathcal{K}}^*(\mathbf{X}) = \frac{1}{d^h}\mathbb{I}_4 \tag{56}$$

where d^h is a measure of the longest diameter of the cell encompassing $\mathbf{X}$. As for the boundary conditions, we use the precomputed displacement of the solid media as the driving Dirichlet boundary conditions for the artificial problem. This has the additional benefit that the interface mesh between the free-space and solid domains (on Γ_0^{ds}) is always synchronised. To ensure the exterior shape of the far-field domain remains the same, we fix all pseudo-elastic degrees-of-freedom on these surfaces. In the case where half of the domain is modelled, as is the case for the problem demonstrated in section 7.2, only symmetry conditions (that is that no out-of-plane displacement may occur) are enforced on the cut-plane.

6 Extension and inflation of a hollow cylinder

In order to illustrate the physical behaviour predicted by the model presented in the preceding sections, we now present some calculations related to standard loading conditions. This section presents a problem of inflation and extension of a magnetoelastic tube that has been solved analytically.

We consider an infinitely long circular cylindrical tube made of an incompressible magnetoelastic material with a directional anisotropy. We work in cylindrical polar coordinates, which in the reference configuration $\mathcal{B}_0$ are denoted by (R, Θ, Z) and in the deformed configuration by (r, θ, z). Let the internal and external radii of the tube in $\mathcal{B}_0$ be given by A and B, which become a and b in $\mathcal{B}_t$ after deformation. The tube is deformed by a combination of inflation and axial stretching as is depicted in figure 5.

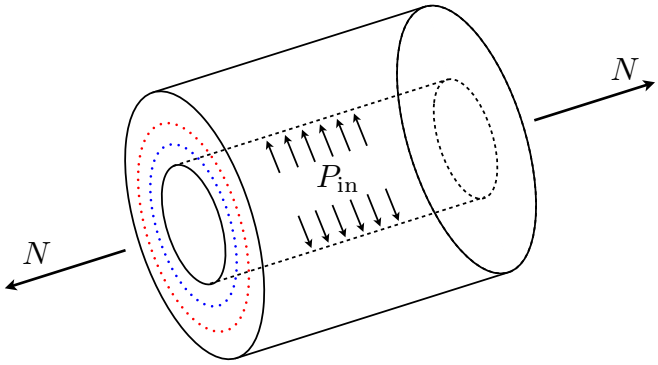

Figure 5: Cylinder being inflated through internal pressure P_{in} and extended in axial direction through force N. Dotted curves in colour denote the direction of average alignment of particle chains and the applied magnetic field.

We will consider the external magnetic field being applied in azimuthal direction by an electric current density through the axis of the tube. In this case, the magnetic field in the azimuthal direction decays with increasing distance from the axis and is given by $h_\theta = h_0/r$ where r is the radius.

The deformation is given (due to incompressibility) by

$$r = \left[a^2 + \lambda_z^{-1}\left[R^2 - A^2\right]\right]^{1/2}, \quad z = \lambda_z Z, \quad \theta = \Theta, \tag{57}$$

where λ_z is the uniform axial stretch. Using the constraint of incompressibility, the principal stretches in the azimuthal and the radial directions are given by

$$\lambda_\theta = \lambda = \frac{r}{R}, \quad \lambda_r = \lambda^{-1}\lambda_z^{-1}, \tag{58}$$

respectively. For this case, the deformation gradient is given by $\mathbf{F} = \text{diag}(\lambda_r, \lambda_\theta, \lambda_z)$.

6.1 Energy density functions

Following the discussion in section 4.2, the energy density function is additively decomposed into the energy of the matrix phase and that of the chain phase. We consider the following prototype functions for each of these components

$$\Omega_0^{\text{mat}} = \underbrace{\frac{n_1}{\alpha}\left[\exp\left(\alpha\left[\mathbf{C}:\mathbf{I}-3\right]^2\right)-1\right]}_{\Omega_0^{m,E}} + \underbrace{n_2[\mathbb{H}\otimes\mathbb{H}]:\mathbf{I} + n_3[\mathbb{H}\otimes\mathbb{H}]:\mathbf{C}^{-1}}_{\Omega_0^{m,ME}}, \tag{59}$$

$$\Omega_0^{c} = \underbrace{\frac{n_4}{\alpha}\left[\exp\left(\alpha[\mathbf{C}^c:\mathbf{I}-\mathbf{G}^2:\mathbf{I}]^2\right)-1\right]}_{\Omega_0^{c,E}} + \underbrace{n_5[\mathbb{H}^c\otimes\mathbb{H}^c]:\mathbf{I} + n_6[\mathbb{H}^c\otimes\mathbb{H}^c]:\mathbf{C}^{-1}}_{\Omega_0^{c,ME}}. \tag{60}$$

The magnetoelastic component is quadratic in terms of the spatial magnetic field vector, and the use of the Fung-type energy function for the elastic part ensures that the chains are stress-free in the undeformed configuration.

In the case of incompressibility $\widetilde{\mathbf{C}} = \mathbf{C}$ and we need only consider the functions provided in equation (59) and equation (60). For such a case, the constitutive relation for the Piola–Kirchhoff stress is given as

$$\begin{aligned}\mathbf{S} = 2\beta_1\mathbf{I} - 2n_3[\mathbf{C}^{-1}\cdot\mathbb{H}]\otimes[\mathbf{C}^{-1}\cdot\mathbb{H}] + 2\beta_2\kappa^2\mathbf{I} + 2\beta_2[1-\kappa][1-3\kappa]\overline{\mathbf{M}}\otimes\overline{\mathbf{M}} \\ -2n_6[\mathbf{C}^{-1}\cdot\mathbb{H}^c]\otimes[\mathbf{C}^{-1}\cdot\mathbb{H}^c] - p\mathbf{C}^{-1},\end{aligned} \tag{61}$$

where

$$\beta_1 = 2n_1\left[\mathbf{C}:\mathbf{I}-3\right]\exp\left(\alpha\left[\mathbf{C}:\mathbf{I}-3\right]^2\right), \tag{62}$$

$$\beta_2 = 2n_4[\mathbf{C}^c:\mathbf{I}-\mathbf{G}^2:\mathbf{I}]\exp\left(\alpha[\mathbf{C}^c:\mathbf{I}-\mathbf{G}^2:\mathbf{I}]^2\right). \tag{63}$$

The magnetic induction is given by

$$\mathbb{B} = -2n_2\mathbb{H} - 2n_3\mathbf{C}^{-1}\cdot\mathbb{H} - 2n_5\mathbf{G}\cdot\mathbb{H}^c - 2n_6\mathbf{G}\cdot\mathbf{C}^{-1}\cdot\mathbb{H}^c. \tag{64}$$

These quantities are given in the spatial configuration as

$$\begin{aligned}\boldsymbol{\sigma} = 2[\beta_1+\beta_2\kappa^2]\mathbf{b} - 2n_3\mathbb{h}\otimes\mathbb{h} + 2\beta_2[1-\kappa][1-3\kappa]\overline{\mathbf{m}}\otimes\overline{\mathbf{m}} \\ -2n_6[\mathbf{b}^{-1}\cdot\mathbf{g}\cdot\mathbb{h}]\otimes[\mathbf{b}^{-1}\cdot\mathbf{g}\cdot\mathbb{h}] - p\boldsymbol{i},\end{aligned} \tag{65}$$

and

$$\mathbb{b} = -2n_2\mathbf{b}\cdot\mathbb{h} - 2n_3\mathbb{h} - 2n_5\mathbf{g}\cdot\mathbf{b}^{-1}\cdot\mathbf{g}\cdot\mathbb{h} - 2n_6\mathbf{g}\cdot\mathbf{b}^{-2}\cdot\mathbf{g}\cdot\mathbb{h}, \tag{66}$$

where we have defined the push-forward of the structure tensor to the spatial configuration as $\mathbf{g} = \mathbf{F}\cdot\mathbf{G}\cdot\mathbf{F}^t$.

It is to be noted here that, due to this particular choice of energy functions, Ω_0^c defined for the particle chain direction results in a Cauchy stress and magnetic induction that are similar to those produced by Ω_0^{mat}, but aligned in the chain direction. The degree of reinforcement in the chain direction is defined by the parameter κ, which measures the strength of anisotropy.

6.1.1 Uniaxial deformation

In order to provide an understanding of the behaviour of the chosen energy density function, we first consider a simple example of uniaxial deformation at a point. The average chain alignment, the applied magnetic field and the applied deformation are all in the same direction, say $\mathbf{e}_1 = \{1,0,0\}^t$. Thus we consider the case when $\mathbf{F} = \text{diag}(\lambda, \lambda^{-1/2}, \lambda^{-1/2})$, $\mathbb{H} = \{H_1,0,0\}^t$, and $\overline{\mathbf{M}} = \{1,0,0\}^t$. For this test case, the total Cauchy stress and the developed magnetic induction in the direction of loading are given by

$$\begin{aligned}\sigma_{11} = 2\left[\beta_1+\beta_2[1+4\kappa^2-4\kappa]\right]\lambda^2 - 2[\beta_1+\beta_2\kappa^2]\frac{1}{\lambda} \\ -2\left[n_3 + n_6[1-2\kappa]^2\frac{1}{\lambda^2}\right]H_1^2,\end{aligned} \tag{67}$$

and

$$\mathbb{b}_1 = -2\left[n_2\lambda^2 + n_3 + [1-2\kappa]^2\left[n_5 + \frac{n_6}{\lambda^2}\right]\right]H_1, \tag{68}$$

where

$$\begin{aligned}\beta_1 =& 2n_1\left[\lambda^2+\frac{2}{\lambda}-3\right]\exp\left(\alpha\left[\lambda^2+\frac{2}{\lambda}-3\right]^2\right),\\ \beta_2 =& 2n_4\left[[1-2\kappa]^2[\lambda^2-1]+2\kappa^2\left[\frac{1}{\lambda}-1\right]\right]\\ &\times\exp\left(\alpha\left[[1-2\kappa]^2[\lambda^2-1]+2\kappa^2\left[\frac{1}{\lambda}-1\right]\right]^2\right).\end{aligned}\tag{69}$$

It is seen from equation (67) that stress increases in general with an increase in the stretch λ. As the dispersion parameter κ increases from 0 to 1/3, the overall magnitude of β_2 decreases for $\lambda > 1$ and increases for $\lambda < 1$ while β_1 remains unaffected. The last term in equation (67) provides a positive stress contribution from the magnetic field for the case when the effective coefficient comprising of the terms n_3 and n_6 is negative. The stress contribution from the magnetic field has a quadratic dependence on H_1 as observed by Varga et al. [66, fig. 6] at least for the case of small strains. Clearly the magnetic contribution to the stress is highest when the chains are perfectly aligned at $\kappa = 0$ and decreases with an increase in the chain dispersion.

The magnetic induction from equation (68) is developed in the same direction as the applied magnetic field when the overall coefficients constituted of the parameters n_2, n_3, n_5 and n_6 are negative. Magnetic induction has a linear dependence on the magnetic field H_1. As κ changes from 0 to 1/3, the magnetic induction decreases in value thus providing maximum response in the case of perfectly aligned chains.

The above stated observations can also be derived from the plots of equations 67 and 68 as shown in figure 6. The graphs are plotted for the values of the parameters listed in table 1 and $H_1 = 2 \times 10^5$ A/m.

Table 1: Baseline values of the material parameters.

μ_0	μ_e	α	n_1, n_4	n_2, n_3, n_5, n_6
$4\pi \times 10^{-7}$ N/A^2	3×10^4 N/m^2	0.15	0.5 μ_e	-0.5 μ_e

The proposed energy function corresponds to a material that shows a much higher resistance to extension in comparison to a compressive deformation as is seen from figure 6a. As observed from figure 6b, a high magnetic induction is developed both during compression and extension when the chains are perfectly aligned. In the case of isotropically distributed particles ($\kappa = 1/3$), the magnetic response during extension is more pronounced in comparison to that during compression.

6.2 Anisotropy in azimuthal direction

We now use the energy density function presented in the previous section to the problem of inflation and extension of a tube as presented in figure 5. As is depicted in figure 5, we consider the average particle-chain alignment to be in the azimuthal direction. Thus,

$$\overline{\mathbf{M}} = \{0, 1, 0\}^t, \qquad \overline{\mathbf{m}} = \mathbf{F}\cdot\overline{\mathbf{M}} = \{0, \lambda, 0\}^t. \tag{70}$$

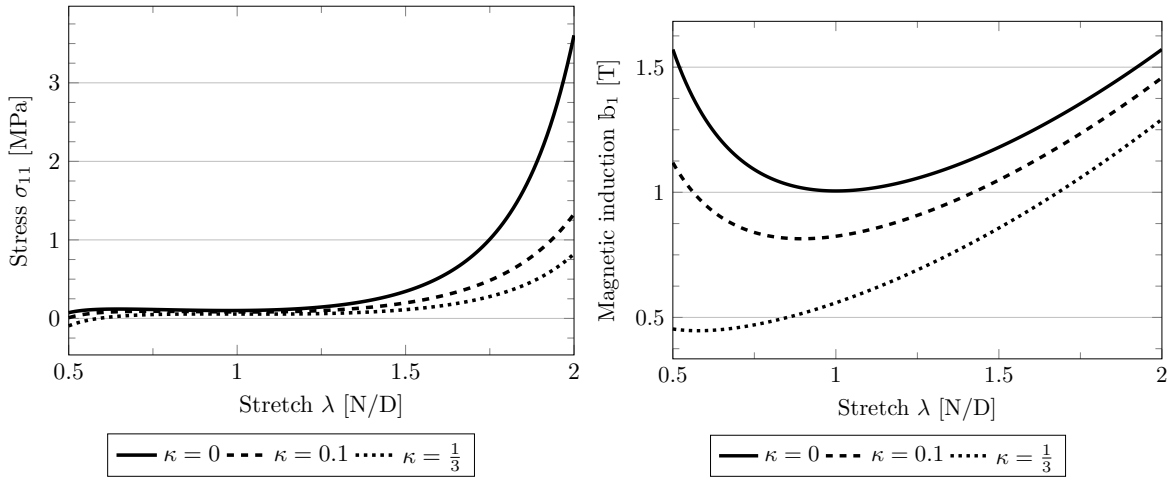

(a) Stress σ_{11} (b) Magnetic induction $\mathbb{b}_1$

Figure 6: Variation of stress and magnetic induction for a uniaxial deformation case for different values of the dispersion parameter κ.

The structure tensor is given by $\mathbf{G} = \text{diag}(\kappa, [1-2\kappa], \kappa)$.

Using the expressions in equation (65), the three principal components of the total Cauchy stress in this case are given by

$$\sigma_{rr} = -p + 2[\beta_1 + \beta_2\kappa^2]\lambda_r^2, \tag{71}$$

$$\sigma_{\theta\theta} = -p + 2\big[\beta_1 + \beta_2\kappa^2 + \beta_2[1-\kappa][1-3\kappa]\big]\lambda^2 - 2n_3h_\theta^2 - 2n_6[1-2\kappa]^2h_\theta^2, \tag{72}$$

$$\sigma_{zz} = -p + 2[\beta_1 + \beta_2\kappa^2]\lambda_z^2, \tag{73}$$

and the azimuthal component of the magnetic induction from equation (66) is expressed as

$$b_\theta = -2n_2\lambda^2h_\theta - 2n_3h_\theta - 2n_5[1-2\kappa]^2\lambda^4h_\theta - 2n_6[1-2\kappa]^2\lambda^2h_\theta. \tag{74}$$

The equilibrium equation $\nabla \cdot \boldsymbol{\sigma} = \mathbf{0}$ gives

$$\frac{d\sigma_{rr}}{dr} = \frac{1}{r}\left[\sigma_{\theta\theta} - \sigma_{rr}\right], \tag{75}$$

$$r\frac{d\sigma_{rr}}{dr} = 2[\beta_1 + \beta_2\kappa^2][\lambda^2 - \lambda_r^2] + 2\beta_2[1-\kappa][1-3\kappa]\lambda^2 - 2n_3h_\theta^2 - 2n_6[1-2\kappa]^2h_\theta^2. \tag{76}$$

Thus the above differential equation can be integrated with respect to r to calculate σ_{rr} as a function of r while $\sigma_{\theta\theta}$ is given as

$$\sigma_{\theta\theta} = r\frac{d\sigma_{rr}}{dr} + \sigma_{rr}. \tag{77}$$

The principal stress in the axial direction (σ_{zz}) can be rewritten, using some algebraic manipulations as

$$\sigma_{zz} = \frac{1}{2r}\frac{d}{dr}(r^2\sigma_{rr}) - \frac{1}{2}[\sigma_{\theta\theta} - \sigma_{rr}] + [\sigma_{zz} - \sigma_{rr}]. \tag{78}$$

Thus the total axial force acting on the cylinder can be computed from

$$N = \int_0^{2\pi}\int_a^b \sigma_{zz}\, r\, dr\, d\theta = \pi\left[a^2 P_{\text{in}} - b^2 P_{\text{out}}\right] + 2\pi \int_a^b \left[\left[\sigma_{zz} - \sigma_{rr}\right] - \frac{1}{2}\left[\sigma_{\theta\theta} - \sigma_{rr}\right]\right] r\, dr. \tag{79}$$

Here P_{in} is the pressure in the inside of the tube ($r < a$) and P_{out} is the external pressure in the region $r > b$. In deriving the above, we have also used the boundary conditions on the lateral surfaces of the tube that are given by the balance of traction as

$$\sigma_{rr} = \sigma^*_{rr} - P_{\text{in}} \quad \text{on } r = a, \qquad \text{and} \qquad \sigma_{rr} = \sigma^*_{rr} - P_{\text{out}} \quad \text{on } r = b, \tag{80}$$

where σ^*_{rr} obtains the value $-\mu_0 h_\theta^2/2$ at $r = a$ and $r = b$. We note that expressions similar to equation (75) and equation (79) have been obtained in the context of magnetoelasticity earlier by Dorfmann and Ogden [20].

The values of the material parameters used to perform the calculations are taken from table 1. The geometry of the tube is taken such that $B/A = 1.4$ while the following values of the applied magnetoelastic deformation are taken

$$\lambda_a = a/A = 2, \quad \lambda_z = 1.5, \quad H_0 = 2 \times 10^5\, \text{A/m}. \tag{81}$$

Here we have defined a reference value H_0 for the azimuthal magnetic field so that at a radius r, h_θ is given by

$$h_\theta(r) = H_0 A/r. \tag{82}$$

We now plot σ_{rr} and $\sigma_{\theta\theta}$ as a function of the non-dimensional radius $\hat{R} = R/A$ in figure 7 for the magnetoelastic coupled loading specified in equation (81) but for different values of κ to observe how the dispersion of chains affects the internal stresses. The radial stress is maximum (a negative value indicating compression) at the inner surface of the tube and decreases along the thickness direction reaching a minimum value close to the outer surface. The circumferential stress is two orders of magnitude higher than the radial stress since both the chains and the applied magnetic field provide reinforcement in this direction. In this case also, the maximum stress occurs at the inner surface which reduces through the thickness with a minimum occurring at the outer surface.

In both the cases, the maximum value of stress is obtained for $\kappa = 0$ when the chains are ideally formed. However, even for a small change (when $\kappa = 0.1$), the response changes rapidly and converges towards that of the matrix ($\kappa = 1/3$).

Given the deformed geometry and the applied magnetic field, one can compute the internal pressure required to maintain the deformation using the boundary condition (80). In figures 8 and 9 we plot the pressure as a function of inflation for two values of λ_z (representing contraction and extension in the axial direction) and three values of the dispersion parameter κ. As expected, the pressure P_{in} increases with the inflation λ_a, with the increase in stiffness being exponential as is a typical response for a Fung type material. The negative values for $\lambda_a < 1$ in the case of $\lambda_z = 0.7$ suggest that an external compressive pressure is required to maintain that geometry. Interestingly very little variation with the value of κ is observed in this region. However, when the tube is in extension ($\lambda_z = 1.5$), the pressure rises both for inflation and deflation when the chains

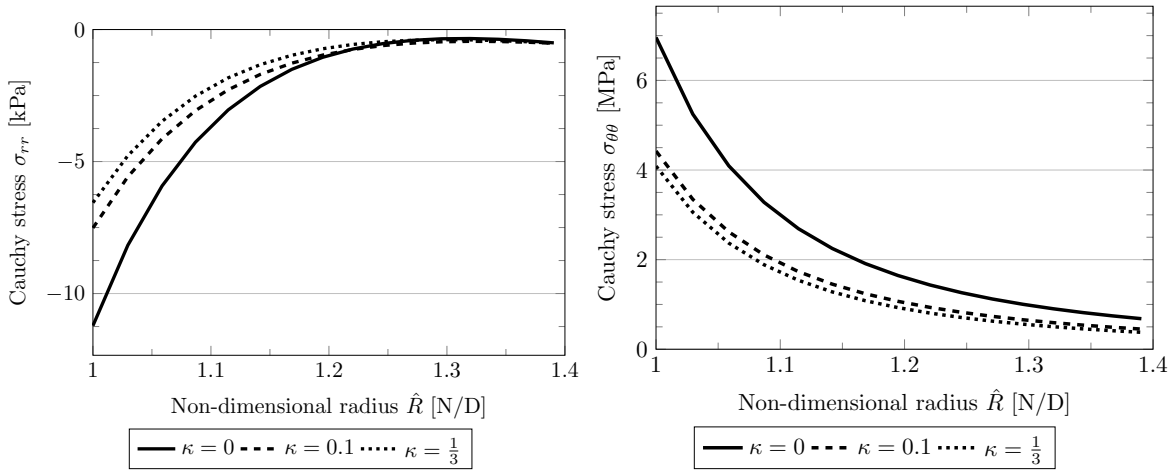

(a) Radial stress σ_{rr} (b) Circumferential stress $\sigma_{\theta\theta}$

Figure 7: Variation of the radial and circumferential stresses along the tube thickness for different values of the dispersion parameter κ.

are fully formed ($\kappa = 0$). This corresponds to a large response of the particle chains to the externally applied azimuthal magnetic field. As inflation reaches higher values ($\lambda_a > 2$) one observes significant differences in the pressure for two extreme values of κ. Similar to the stress response, even a very small dispersion in the chains (e.g. $\kappa = 0.05$) leads to a large change in the required pressure and the response approaches to that of an isotropic magnetoelastic solid.

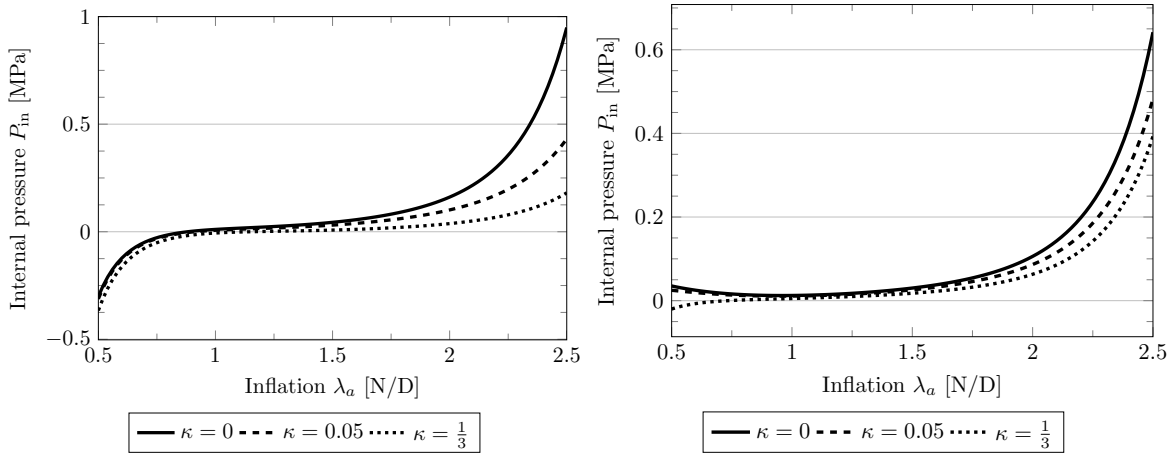

(a) $\lambda_z = 0.7$ (b) $\lambda_z = 1.5$

Figure 8: Internal pressure P_{in} for three values of κ and a prescribed axial stretch.

For the same case, we plot the variation of pressure with the externally applied magnetic field in figure 9 for both inflation and extension ($\lambda_a = \lambda_z = 1.5$). In general, the required internal pressure increases with an increase in the applied magnetic field, leading to the conclusion that an azimuthal magnetic field tends to shrink the tube in radial direction. The required pressure is highest when the chains are perfectly formed and provide reinforcement in the azimuthal direction, and minimum for the isotropic material.

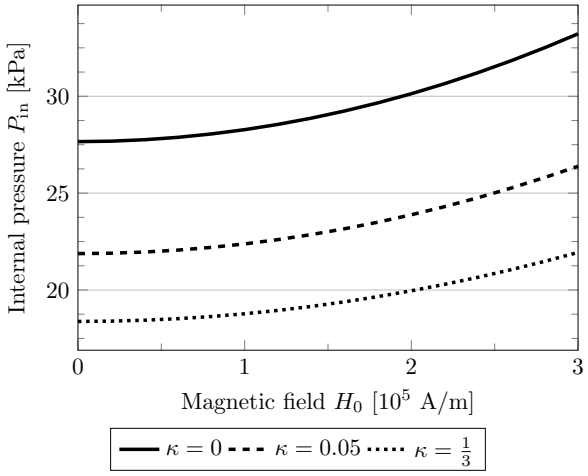

Figure 9: Internal pressure P_{in} for three values of the parameter κ. The deformation parameters were $\lambda_a = 1.5, \lambda_z = 1.5$.

We compute the total axial force per unit area $\hat{N} = N/[\pi[b^2 - a^2]]$ required to maintain the deformed geometry using equation (79) and plot this value in figure 10 to observe the effect of chain dispersion. The applied loading conditions are that $\lambda_z = 1$ and $H_0 = 2\times10^5$ A/m. As the tube is inflated, it tends to shorten in length and an extensional axial force is required to maintain the original length. Thus the force $\hat{N}$ increases with inflation. The axial load is at a minimum in the case of perfect anisotropy when all chains are aligned in the azimuthal direction. As dispersion increases, the particle chains start to provide a contribution in the axial direction and one observes an increase in the axial force necessary to maintain the same level of deformation. Similar to the pressure response, a significant variation with κ is observed only for the case of inflation $\lambda_a < 1$ and not in contraction $\lambda_a < 1$.

7 Finite element examples

The finite element problem has been implemented using a total Lagrangian approach within an in-house code developed using the open-source FE library `deal.II` [1, 2]. The use of continuous linear shape functions for the purpose of discretising the magnetic potential Φ ensure that its gradient is curl-free, thereby satisfying equation $(7)_1$. Similarly, continuous trilinear shape functions chosen for the displacement $\boldsymbol{\varphi}$ ensure that the compatibility conditions for the deformation are naturally satisfied. For the first problem shown in section 7.1, a direct solver, namely UMFPACK [17], was used to solve the linear system of equations given by equation (51). In section 7.2 where a larger geometry is considered, the entire linear system is solved using the stabilised biconjugate gradient method [28] in conjunction with an algebraic multi-grid preconditioner [26, 29].

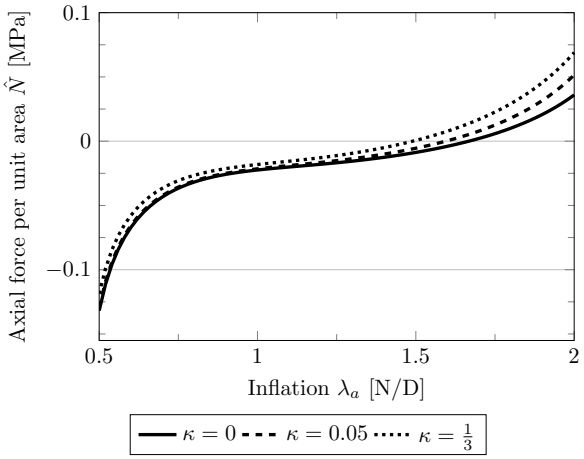

Figure 10: Axial force per unit area $\hat{N}$ [N/m^2] vs the inflation $\lambda_a = a/A$ for three values of the parameter κ.

7.1 Oscillatory pure shear with step increase in magnetic potential

In order to further demonstrate the general and limiting behaviour of the particle chain model, a strip of magnetoelastic material is modelled assuming plane-strain conditions. In this particular example, the free-space has been neglected. With reference to figure 11a, the problem geometry and imposed boundary conditions are as follows: The strip of dimensions $1 \times 3\text{mm}^2$ (discretised by 12×25 finite elements) is fully fixed on the $-\mathbf{e}_1$ face and has a sinusoidally oscillating shear displacement in $\mathbf{e}_2$ direction (constant frequency and amplitude) prescribed on the $+\mathbf{e}_1$ face. The maximum lateral displacement is set at 0.25mm (corresponding to a maximal shear strain of approximately 25%), with four periods simulated. Due to the plane-strain condition, the material thickness was arbitrarily chosen to be 0.1mm and discretised by only a single finite-element. Note that as the material has no rate dependence, the problem remains quasi-static in nature and time can be interpreted as a loading parameter. The $\pm\mathbf{e}_2$ faces are traction-free and periodic displacement conditions are adopted on the $\pm\mathbf{e}_3$ surfaces to ensure that the plane-strain condition is achieved. The magnetic field is induced by prescribing a step-wise increasing potential difference $\Delta\Phi$ between the upper and lower surfaces of the strip. The chain average orientation $\overline{\mathbf{M}}$ is defined by the angle θ, which describes the offset with respect to the thickness direction $\mathbf{e}_1$. As is illustrated in figure 11b, from this configuration it is expected that the tensile and compressive behaviour of magnetised particle chains can be evaluated. For this purpose, measurement data is recorded at the geometric centre of the strip (denoted by point $\mathbf{P}$) to minimise the influence of the boundaries.

In this example, the energy density function nominally remains that presented in equations (59) and (60) but is augmented by the polyconvex volumetric function [30]

$$\Omega_0^{\text{vol}} = \frac{\gamma}{4}\left[J^2 - 1 - 2\ln J\right], \tag{83}$$

where γ represents the bulk modulus. The material parameters for this problem are the same as given in table 1 with the addition that $\gamma = 2.9 \times 10^5$ N/m^2.

The observed magnetic behaviour of the material with strong chain-like structures

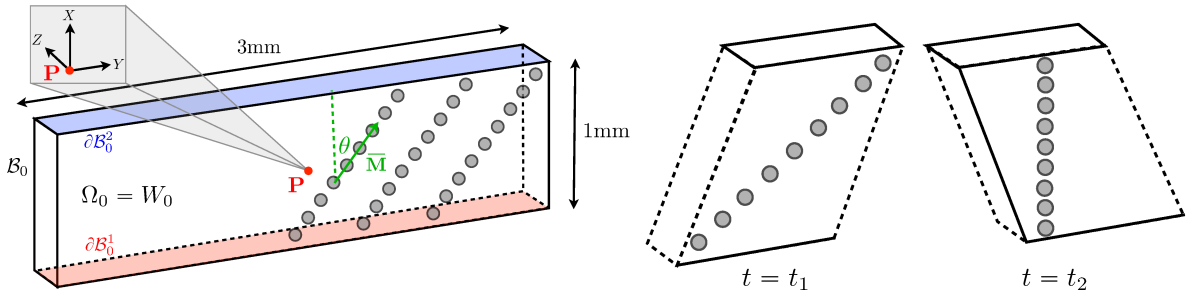

(a) Material configuration with boundary conditions. For this problem, $\mathcal{D}_0 \cap \mathcal{S}_0 = 0$.

(b) Illustration of offset chain deformation upon deformation

Figure 11: Problem description, boundary conditions and expected behaviour of microstructure. The upper surface $\partial\mathcal{B}_0^2$ undergoes oscillatory displacement $\mathbf{u} = \overline{u}\,(t)\,\mathbf{e}_2$, while a magnetic potential difference between the upper and lower surfaces is prescribed. When the material is sheared to the right, chains will be placed in tension. When the material is sheared to the left, (offset) chains may experience compression.

differed greatly to that of an isotropic medium. For both cases, away from the traction-free boundaries and regardless of the motion, the magnetic field (related to the primary field Φ) remains vertically aligned between the upper and lower surfaces. However, the predicted magnetic induction upon incorporation of the particle chain model is no longer aligned with the magnetic field, but rather reorientated towards the direction of the particle chains. Furthermore, the direction of the total magnetic induction is measurably influenced by the deformation as the particle chains undergo length change and rotation.

7.1.1 Variation of dispersion parameter κ

Firstly, we demonstrate the effect of the dispersion parameter κ on the material behaviour for a fixed chain orientation $\theta = 0°$. The history of the component of the true stress aligned in the thickness direction for the elastic components of the stored energy function is plotted in figure 12 for one full period of deformation. It is shown that elastic stresses produced in the chain phase increase towards that of the matrix contribution as the dispersion is reduced. When the particles are randomly dispersed, the chain stress is negligible. It is observed that in the limiting case of $\kappa = 0$, the chain stress exceeds that of the matrix as the effective chain stretch computed from $\mathbf{C}^c : \mathbf{I} - \mathbf{G}^2 : \mathbf{I} = \lambda_c^2 - 1$ is greater than the matrix exponent $\mathbf{C} : \mathbf{I} - 3 = \lambda_1^2 + \lambda_2^2 + \lambda_3^2 - 3$ for which $\lambda_2 < 1, \lambda_3 = 1$. Furthermore, due to their alignment, the stress contributions σ_{11} suggests that only tensile deformation has occurred within the particle chains.

Similarly, the stress contribution from the magnetoelastic components of the chain energy function increases as the value of the dispersion parameter is reduced. Figure 13a also highlights that the chain magnetoelastic stresses are proportional to the square of the spatial magnetic field magnitude and, for this chain orientation, are unaffected by the deformation. Contrary to the previous result, for near perfectly developed particle chains, the chain and matrix stresses are equal. The stress magnitude is reduced considerably as the degree of anisotropy is lowered, but the chains remain effective force generators for relatively large values of κ. A similar trend is observed in the magnetic induction generated though the thickness direction and shown in figure 13b.

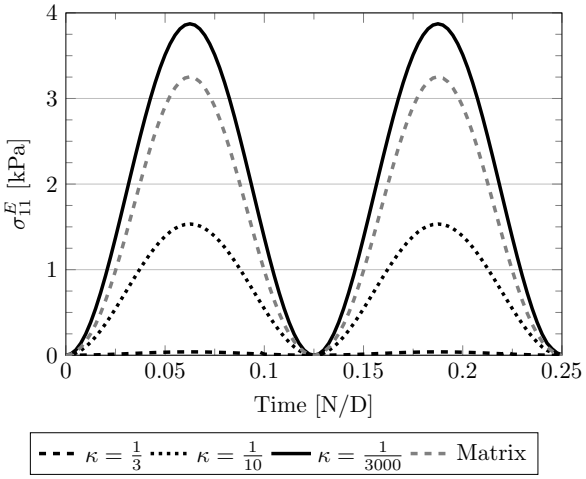

Figure 12: Variation of chain dispersion parameter. Cauchy stress magnitude in the $+\mathbf{e}_1$ direction (aligned with chain reference direction) for elastic components (matrix, chain) of the energy density function. As the stress in the elastic components is dependent only on the deformation, results for a single full oscillation are shown. The values for the matrix component were recorded for the case for which $\kappa = \frac{1}{3000}$, and the time scale has been non-dimensionalised.

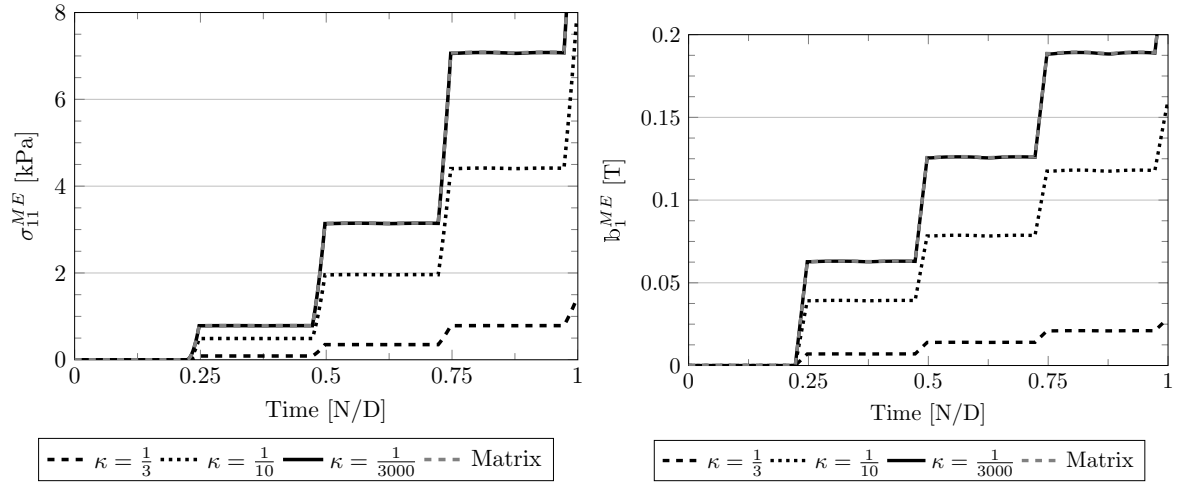

(a) Cauchy stress σ_{11} (b) Spatial magnetic induction $\mathbb{b}_1$

Figure 13: Variation of chain dispersion parameter. Cauchy stress and spatial magnetic induction magnitude in the $+\mathbf{e}_1$ direction (aligned with chain reference direction) for magnetoelastic components of the energy density function. Within the given time-frame, four full periods of mechanical oscillation and three ramped increases in the scalar potential difference take place. Note that the results for the matrix and $\kappa = \frac{1}{3000}$ are near identical.

7.1.2 Chain orientation

We now consider a variable chain orientation by changing the value for θ while maintaining a constant dispersion parameter $\kappa = \frac{1}{3000}$. As is illustrated in figure 11b, it is now expected that chains may experience both tensile and compressive deformation during loading.

This precise behaviour is observed in figure 14. Introducing an angular offset produces tensile stresses in the chain for the first half-period of deformation, while compression is experienced during the second half. Due to the geometry of the problem, the peak value of the measured component of the stress is greater in magnitude during tension than compressive loading of the chains. For $\theta = 30°$, the chains are nearly aligned with the direction of principal stretch, invoking the largest stress response of the tested cases. As the chains become more horizontally aligned, they undergo less deformation and exhibit lower stresses. In the limiting case of $\theta = 90°$, there is no contribution to the stress from the chains.

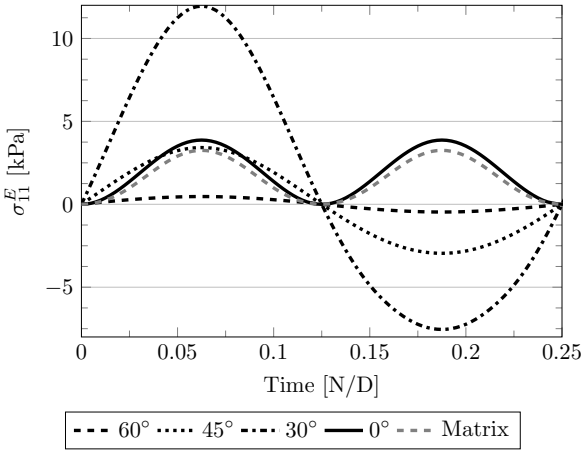

Figure 14: Variation of chain orientation. Cauchy stress magnitude in the $+\mathbf{e}_1$ direction (aligned with chain reference direction) for elastic components (matrix, chain) of the energy density function. The values for the matrix component were recorded for the case for which $\theta = 0°$.

As is shown in figure 15a, a similar dependence on deformation is observed for the magnetoelastic contributions to the stress. Significant deformation of the chains produces a deviation of the value of stress away from a mean value (computable at $\mathbf{F} = \mathbf{I}$). Due to the form of the energy function (specifically its dependence on $\mathbf{C}^{-1}$), the generated magnetoelastic stress is reduced when the chains are stretched, and increased when they are shortened. From a microscopic viewpoint, this is sensible as for the most part the closer the magnetisable particles are to one another, the larger their force-generation properties are. This variance in stress is again greatest when the chains are most aligned with the direction of principal strain.

Similar trends are observed for the magnetic induction shown in figure 15b. Increasing the offset angle reduced contribution from the magnetoelastic components of the energy density function to the first component of the magnetic induction. These contributions were also influenced by the chain stretch. Comparing figure 15a to figure 15b, it is observed that the magnetoelastic contribution to the stress, which is dependent on $|\mathbb{h}^c|^2$, is significantly more sensitive to the chain orientation than that of the magnetic induction, which has a linear dependence on $\mathbb{h}$.

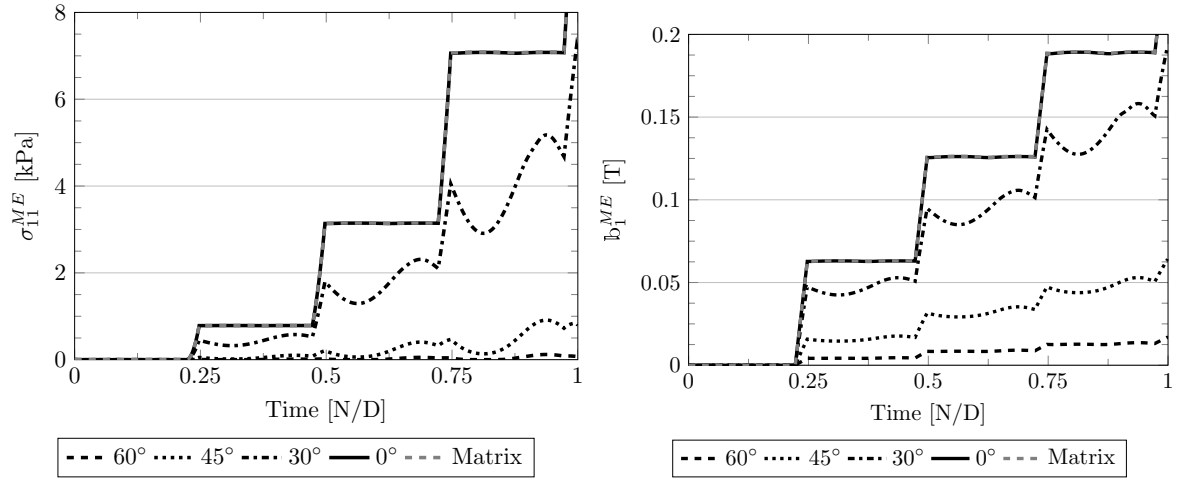

(a) Cauchy stress σ_{11} (b) Spatial magnetic induction $\mathbb{b}_1$

Figure 15: Variation of chain orientation. Cauchy stress and spatial magnetic induction magnitude in the $+\mathbf{e}_1$ direction (aligned with chain reference direction) for magnetoelastic components of the energy density function. Note that the results for the matrix and $\theta = 0°$ are near identical.

7.2 Tube with helical arrangement of chains in magnetic field

In this example, we examine the practical implication of being able to resolve the mechanical and magnetic properties of particle chains, versus the behaviour of its surrounding matrix. Shown in figure 16a, a thick-walled tube (denoted $\mathcal{B}_0$) of magneto-sensitive material, with dimensions $D_i = 1$mm, $D_o = 2$mm, $L = 2.5$mm and a fillet radius of $R_f = 0.25$mm, is placed within a magnetic field. The tube is axially centred in the overall domain $\mathcal{D}_0$ and its one surface is aligned with the $-\mathbf{e}_3$ end-surface of $\mathcal{D}_0$. The overall diameter and length of the computational domain are $D_\infty = 6$mm and $L_\infty = 5$mm respectively. A point of measurement $\mathbf{P} = (0, 0.75, 2.25)$mm is located halfway between the inner and outer radii and near the end of the tube exposed to the free-space. The symmetric problem discretisation is depicted in figure 17 with the filleting at the one end of the tube, necessary to ensure that there exist no magnetic singularities in the problem, clearly visible. The magneto-elastic media is represented by 9728 cells, and the free-space by 25280 cells. The aforementioned choice of finite-element shape-functions results in a total of 36960 elastic and 36576 potential degrees-of-freedom for the boundary value problem.

The magnetic field is generated by the prescription of an increasing magnetic potential difference $\Delta\Phi$ (to a maximum difference of 250A, the limit of numerical stability for some of the reported cases) between the axial surfaces of $\mathcal{D}_0$. The radial extents of $\mathcal{S}_0$ have no prescribed potential, and are therefore subject to the natural boundary condition $\mathbb{B}_\infty \cdot \mathbf{N}_\infty = 0$. Displacement constraints are enforced on the end-surface of $\mathcal{B}_0$ that intersect with the domain boundary. In particular, no axial movement is allowed in this plane with the additional constraint that the outer annulus of the tube is fully fixed. Lastly, as is illustrated in figure 16b, a spatial traction boundary condition $\mathbf{t}_a(\mathbf{x}) = -\lambda[\mathbf{u} \cdot \mathbf{e}_r]\,\mathbf{e}_r$ is set on the radial surface of the tube to penalise the radial dilation or contraction of this surface. Here, the direction vector $\mathbf{e}_r$ is the radial projection of the

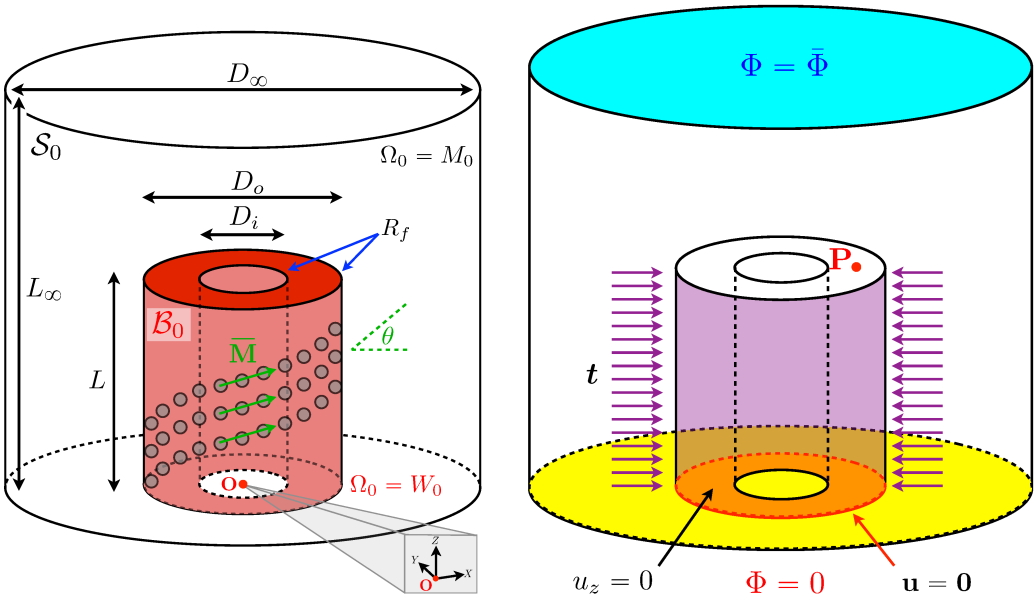

(a) Material configuration with helical chain structure of MRE highlighted

(b) Boundary conditions imposed on domain

Figure 16: Problem description, boundary conditions and orientation of microstructure. In this illustration, the chains are aligned at 45° to the circumferential direction. Except for the outer annulus that is completely fixed, the bottom of the tube is free to slide in the XY plane. An increasing potential difference is applied between the very upper and lower surfaces of the domain. The tube is filleted on the edges indicated by R_f. The measurement point **P** is near the free end of the tube and midway between the inner and outer radial surfaces.

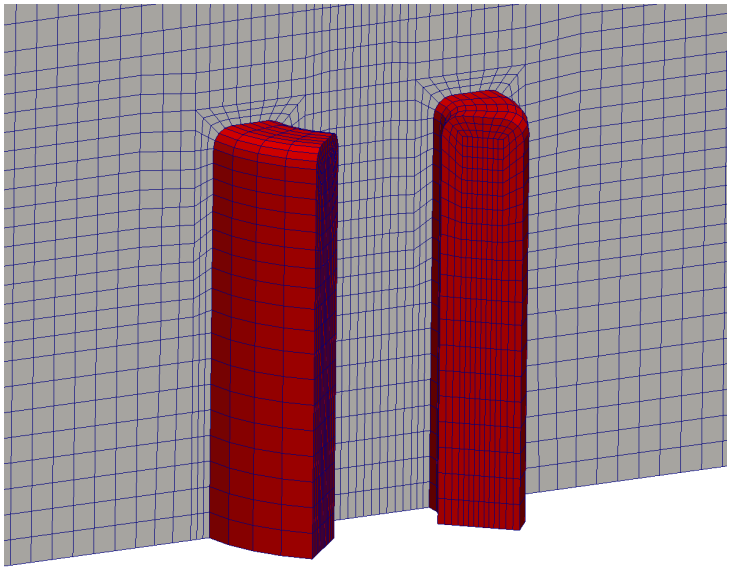

Figure 17: Sectioned view of the tube ($\mathcal{B}_0$, red) and surrounding free-space ($\mathcal{S}_0$, grey) illustrating the spatial discretisation.

current position $\mathbf{x} = \boldsymbol{\varphi}(\mathbf{X})$ onto the original tube outer surface, and the value of the penalty parameter $\lambda = 250\text{N/mm}^3$. As the integration of the traction was performed on the reference domain, we define an equivalent Cauchy stress such that $\mathbf{t}_a(\mathbf{x}) = \boldsymbol{\sigma} \cdot \mathbf{n} \equiv [\mathbf{t}_a \otimes \mathbf{n}] \cdot \mathbf{n}$. Thereafter, Nanson's formula is used to define $\mathbf{t}_A$, the equivalent referential traction, such that $\mathbf{t}_A \, \mathrm{d}A = \mathbf{t}_a \, \mathrm{d}a = [\mathbf{t}_a \otimes \mathbf{n}] \cdot J\mathbf{F}^{-t} \cdot \mathbf{n} \, \mathrm{d}A$. The linearisation of the variation of the total potential energy, given in equation (43), was augmented with the additional non-symmetric term

$$\Delta\delta\Pi^{\text{ext}} = -\int_{\Gamma_0^t} \delta\mathbf{u} \cdot \left[\frac{\partial \mathbf{t}_a}{\partial \mathbf{u}} \cdot \Delta\mathbf{u} + \frac{\partial \mathbf{t}_a}{\partial \mathbf{F}} \cdot \Delta\mathbf{F} \right] \tag{84}$$

to account for the deformation-dependent traction and normal.

The tube is composed of a media similar to that used in section 7.1, with the exception that we substitute an incompressible neo-Hookean material

$$\Omega_0^{m,E} = \frac{\mu_e}{2} \left[\overline{I}_1 - 3 \right], \tag{85}$$

where μ_e is the shear modulus, for the elastic part of the matrix energy density function previously described in equation (59), and additionally utilise the volumetric energy function provided in equation (83). The baseline material coefficients[2] are given in table 2.

Table 2: Baseline values of the material parameters.

μ_e	γ	α	n_2, n_5	n_3, n_6
30kPa	1490kPa	1	$0.5\mu_0$	$-\mu_0$

For this problem, we identify the material parameter $n_4 = \frac{\mu_c}{2}$ as being related to the small-strain chain shear modulus. The particle chains are assumed to, in the general case, be arranged in a helical formation within the media. The chain or helix angle θ is given with respect to the point-wise azimuthal tangent vector $\mathbf{e}_\theta$, such that the average chain direction $\overline{\mathbf{M}} = \overline{\mathbf{M}}(\mathbf{X})$. The baseline chain parameters are listed in table 3.

Table 3: Baseline values of the chain parameters.

κ	θ	$\frac{n_4}{\mu_e}$
$\frac{1}{3000}$	45°	$\frac{1}{10000}$

A typical result of the fields for the magnetic quantities is presented in figures 18 and 19. The magnetic field is aligned axially with the tube, with a strength weaker than

[2] Numerical issues related the presence of a non-negligible Maxwell stress contribution have been indicated previously [14]. As a first approximation, it is sometimes convenient to ignore the Maxwell contributions [53]. For this problem of a compliant elastomer in the presence of a strong magnetic field, a large bulk modulus γ was required in order to maintain numerical stability. However, the use of linear displacement ansatz to represent quasi-incompressible media in some scenarios may lead to artificial volumetric locking behaviour being exhibited [33]. Comparison of a selection of the results presented later with those derived using higher-order finite-elements produced, in the worst case, displacement fields with less than 8% difference between them. This suggested that the problem, while completely fictitious, nonetheless remained locking free.

that of the far-field value present in the bulk of the material. A significant perturbation in the scalar potential gradient is present at the end of the tube, ensuring that equation $(7)_2$ is satisfied. If there exists no particle chains, or $\overline{\mathbf{M}}$ is aligned perpendicular to the applied magnetic field, then the resulting magnetic induction is aligned with $\mathbb{h}$. However, as is shown in figure 18c, the magnetic induction is offset towards $\overline{\mathbf{M}}$ should the dispersion parameter be sufficiently low. With the chosen material coefficients the tube compresses axially and expands radially inwards. In figure 19b it is shown that the presence and alignment of the mechanically weak chains generate additional forces that not only further shorten the tube, but also induces a significant degree of torsion in it.

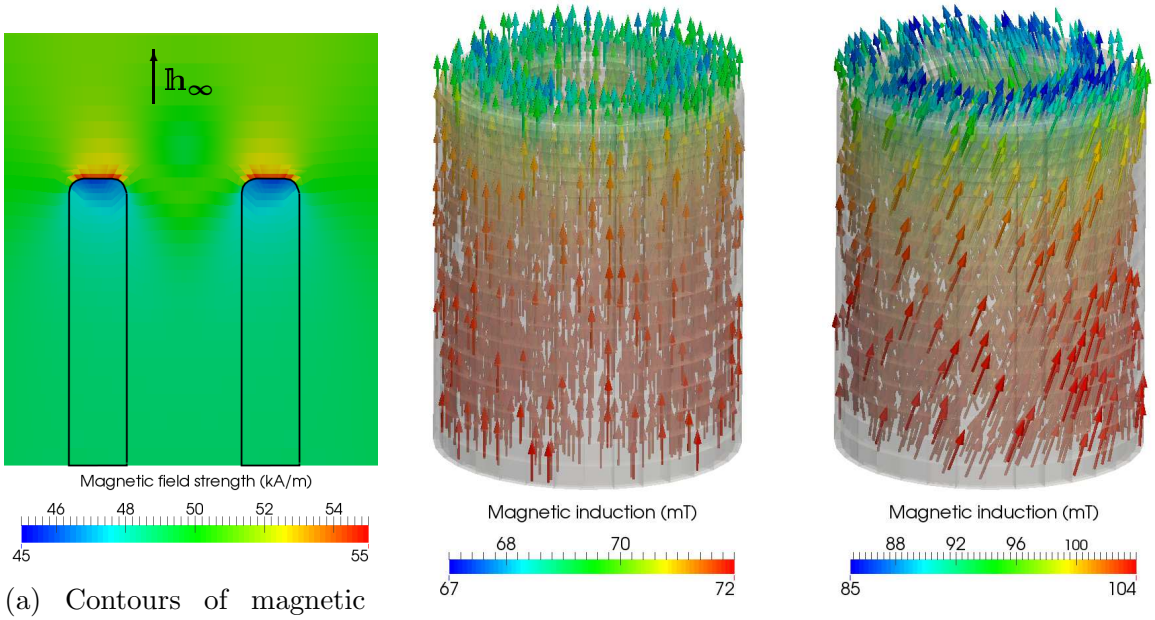

(a) Contours of magnetic field strength. The black lines outline the cross-section of the tube.

(b) Magnetic induction (either without particle chains, with $\kappa = \frac{1}{3}$ or with $\theta = 0°$)

(c) Magnetic induction (with particle chains; parameters given in table 3)

Figure 18: Magnetic quantities (shown in $\mathcal{B}$) at maximum scalar potential difference. The direction of the far-field magnetic field is indicated in figure 18a.

Hereafter, in a parametric study we investigate the influence of various material parameters on the displacement recorded at $\mathbf{P}$.

7.2.1 Variation of dispersion parameter

The introduction of the helically orientated particle chains of sufficient consistency significantly influence the mechanical response of the magneto-sensitive tube. As was previously described, magnetostriction of the media is induced by application of the magnetic field. However, if the chains are strongly formed, twist can be also induced in the tube. Given that the material remains compliant in the direction of the chains, the chains shorten significantly in the direction of $\overline{\mathbf{M}}$ thereby causing rotation of the material.

Figure 20 quantifies the resulting twist and shortening recorded at $\mathbf{P}$ under increasing magnetic load. For the chosen material models, parameters and boundary conditions, the total displacement and magnetic field strength are quadratically related. Although the

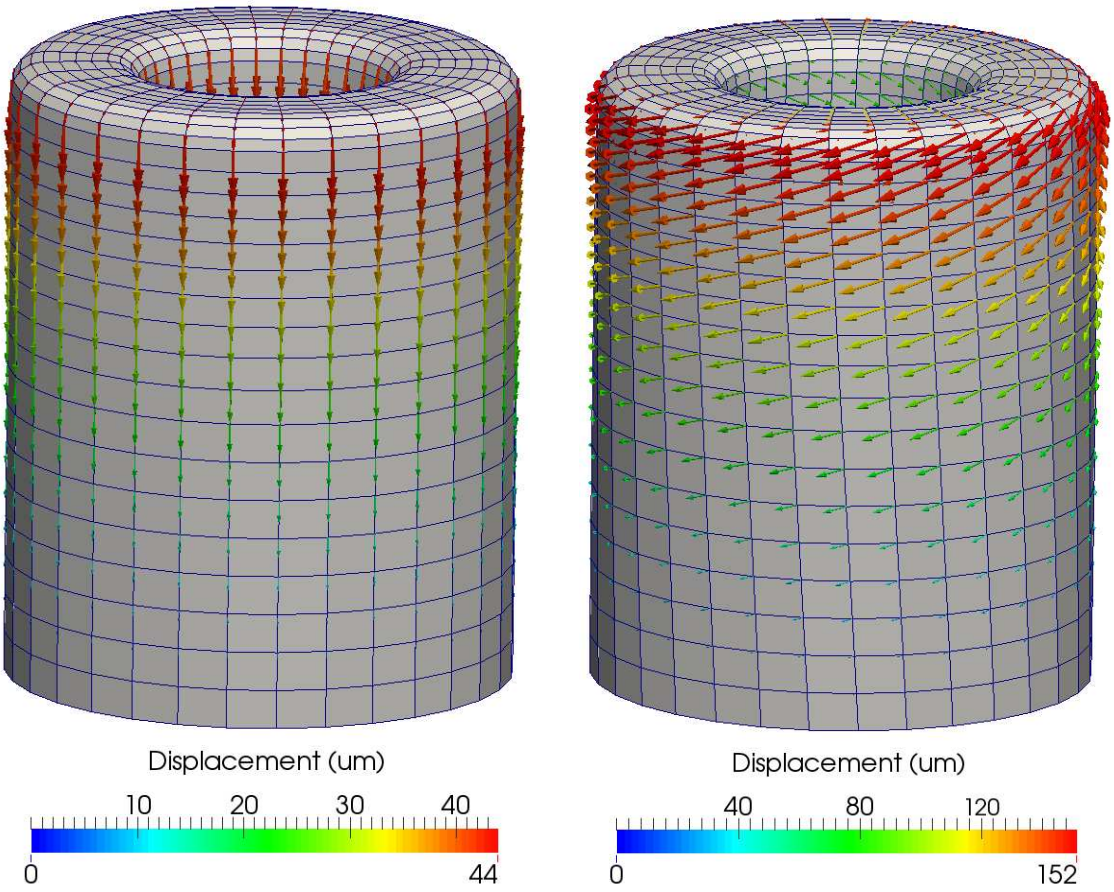

(a) Displacement field either without particle chains, with $\kappa = \frac{1}{3}$ or with $\theta = 0°$

(b) Displacement field with particle chains (parameters given in table 3)

Figure 19: A comparison of the displacement fields generated by ignoring or including the influence of particle chains. Vectors are coloured and scaled relative to the magnitude of the displacement.

total twist is directly proportional to the dispersion parameter, the overall reduction in length of the specimen remains largely independent of κ. Associated with the decrease in the dispersion parameter is a marginal stiffening upon deformation in the axial direction. This is not completely offset by the increase in force generation properties in the axial direction and therefore leads to decreased shortening of the tube. It should be noted that a significant twist is measured even when the particles constituting the chains are not highly organised.

7.2.2 Variation of chain orientation

The chain orientation influences not only the degree of magnetisation of the particle chains, but also the line of action of the resulting force developed due to particle-particle interactions. It is demonstrated visually in figure 21 that modification of the orientation angle, for strongly formed but compliant chains, affects both the amount of twist and contraction induced in the tube.

Interestingly, as can be deduced from figure 21a, there exists some non-trivial optimal

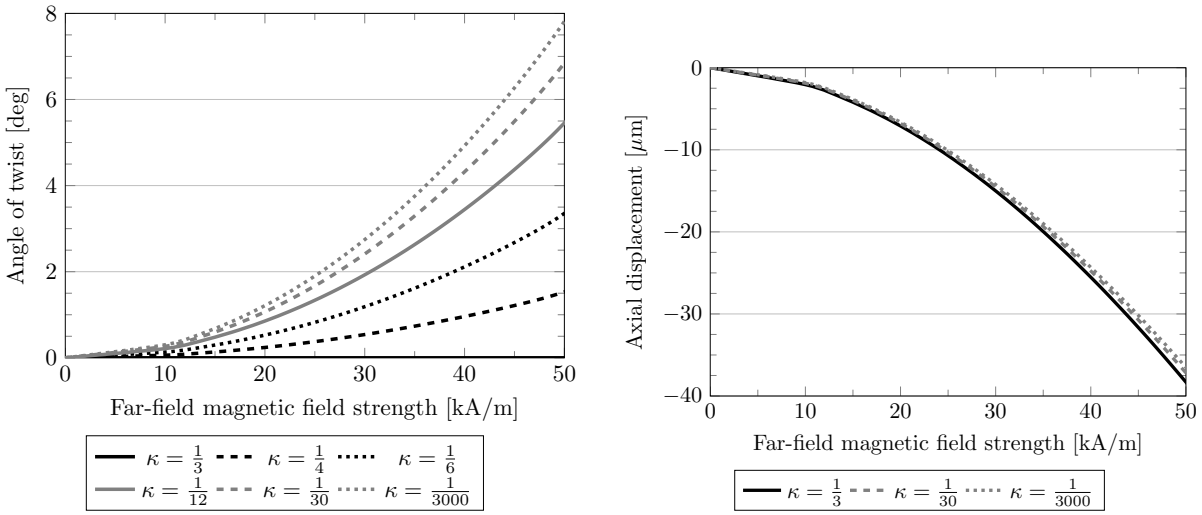

(a) Angle of twist (b) Axial displacement

Figure 20: Influence of dispersion parameter on deformation at measurement point **P** when the chains are mechanically weak ($\frac{n_4}{\mu_e} = \frac{1}{10000}$). We consider the deformation field shown in figure 19b to have undergone positive angle of twist.

value for θ such that the amount of twist is maximised. For the tested range of parameters, the choice of $\theta = 60°$ induced the largest angular displacement in the sample at point **P**. Figure 21b however demonstrates that the total axial contraction depends on the cosine of θ. When the chains are aligned with the direction of the magnetic field, they reinforce the magnetostrictive effect of the matrix, resulting in the greatest shortening effect. With the chains perpendicular to the magnetic field, they remain non-magnetised and no chain magnetisation stress is generated. They do however still affect the mechanical stiffness of the material in the azimuthal direction.

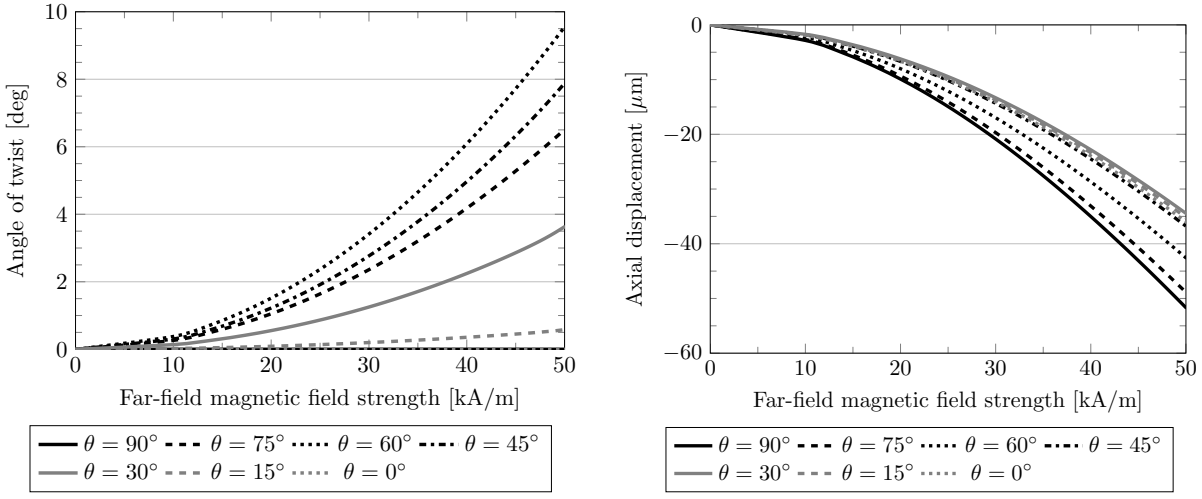

(a) Angle of twist (b) Axial displacement

Figure 21: Influence of chain orientation on deformation at measurement point **P**.

7.2.3 Variation of chain elastic modulus

Previously the examined conditions were such that $\mu_c \ll \mu_e$, inferring that the chains provide little mechanical reinforcement to the material. However, given that the typical composition of such a material involves the ordered deposition of metallic particles in a soft substrate, it is more likely that in commercially applicable materials the difference between μ_c and μ_e is less extreme and $\mu_c \geq \mu_e$. The actual ratio of these effective shear moduli not only depends on the particulate composition, but also the inter-particle space occupied by the compliant matrix. Towards the limit when $\mu_c \gg \mu_e$, it can be assumed that the micron-sized particles are in contact and effectively form very stiff reinforcing chains.

As is shown in figure 22, the ratio of the chain to matrix shear modulus plays a significant role in the deformation of the tube resulting from magnetic loading alone. It is observed that when the chain shear modulus is very large in comparison to that of the matrix, the induced direction of twist is opposite to that caused when the chains are compliant. This is as the increased stiffness in chain direction ensures that direction of deformation is locally restricted primarily to transverse plane of isotropy. Associated with this increase in chain stiffness is a reduction in the total twist and axial shortening. When this ratio of stiffnesses is $\dfrac{\mu_c}{\mu_e} = 2\dfrac{n_4}{\mu_e} \approx 10$, the magnetically-generated contractile force in the circumferential direction is nearly perfectly balanced by the additional stiffness provided by the particle chains in this direction.

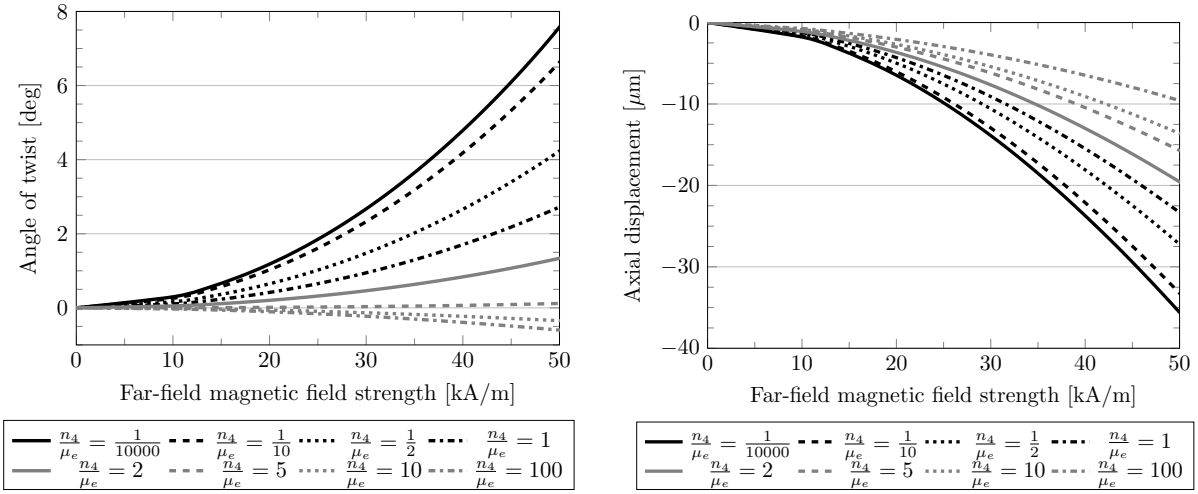

(a) Angle of twist (b) Axial displacement

Figure 22: Influence of chain shear modulus on deformation at measurement point **P**.

Given that the influence of the chain stiffness has such a significant impact on the material deformation, we revisit the scenario described in section 7.2.1, but now prescribe mechanically stiff chains. Figure 23 illustrates that a decrease in the dispersion parameter is associated with a notable decrease in axial shortening due to the increased material stiffness. However, contrary to what has been observed previously, it is also correlated with a decrease in the amount of (negative) twist induced in the tube. At some non-trivial value of κ (which has not been resolved here), the force-generation properties of the relatively dispersed chain structures overcome the mechanical reinforcement. However,

as the chains become less dispersed the angular displacement of the tube is reduced significantly due to the increased stiffness in the circumferential direction.

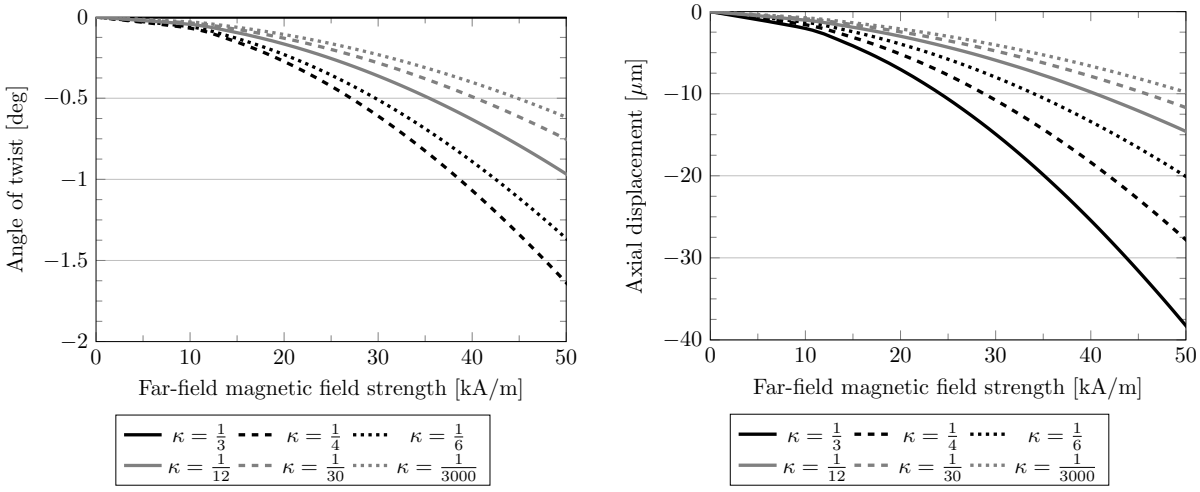

(a) Angle of twist (b) Axial displacement

Figure 23: Influence of dispersion parameter on deformation at measurement point **P** when the chains are mechanically stiff ($\frac{n_4}{\mu_e} = 100$).

7.2.4 Variation of bulk and chain material coefficients

Depending on the experimental conditions and organisation of the particle micro-structure developed during curing, the MRE may be expected to demonstrate different material behaviour [16, 65], namely axial contraction or elongation. The former effect has been shown thus far, but in this section we will demonstrate that modification of the magneto-elastic material coefficients used in table 2 for the prototype energy function causes the material to exhibit different behaviours. In each instance, we vary both the chain and bulk magneto-static and magneto-elastic material coefficients[3] (by setting $n_2 + n_3 = n_5 + n_6 = -0.5\mu_0$) such that the magnetic induction within the material remains qualitatively and quantitatively similar.

In figure 24 the outcome of using the material coefficients listed in table 4 are illustrated. It is apparent both axial contraction and elongation of the tube can be modelled using the energy density function. With reference to Danas et al. [16, fig. 5], the choice of chain material coefficients is assumed to be linked to the microstructure and therefore dictate their magnetostrictive behaviour. In case 7, the magneto-elastic component is removed, with no twist being induced and axial extension of the tube occurring due to the influence of the free-space Maxwell stress. In contrast to the previous results and those demonstrated in cases 1–6, positive values for n_6 cause the chains to elongate and induce a negative angle of twist.

Figure 25 demonstrates that an alteration of the coefficients governing the chain behaviour can significantly alter that behaviour of the tube under a magnetic field. For the

[3] Note that the convexity/concavity of the energy density function has not been examined.

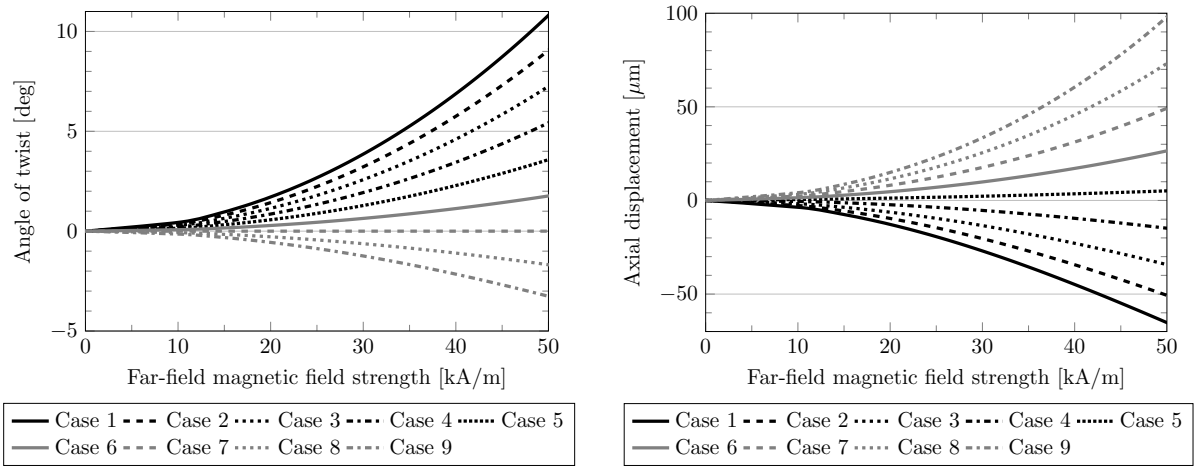

(a) Angle of twist

(b) Axial displacement

Figure 24: Influence of material coefficients on deformation at measurement point **P** when the chains are mechanically weak ($\frac{n_4}{\mu_e} = \frac{1}{10000}$). The material coefficients for each case are listed in table 4.

Table 4: Chain and bulk material coefficients for cases in parameter study where $n_2 = n_5$ and $n_3 = n_6$.

Case	n_2, n_5	n_3, n_6	Case	n_2, n_5	n_3, n_6
1	μ_0	$-1.5\mu_0$	6	$-0.25\mu_0$	$-0.25\mu_0$
2	$0.75\mu_0$	$-1.25\mu_0$	7	$-0.5\mu_0$	0
3	$0.5\mu_0$	$-\mu_0$	8	$-0.75\mu_0$	$0.25\mu_0$
4	$0.25\mu_0$	$-0.75\mu_0$	9	$-\mu_0$	$0.5\mu_0$
5	0	$-0.5\mu_0$			

parameters listed in table 5, the axial deformation trends remain qualitatively similar to those shown in figure 24. However, the force generation properties of the chains differ and, in some cases, the chain model no longer produces a force that reinforces the bulk model leading to smaller displacements. This can be verified by comparing the twist directions between the two sets of results. For comparable bulk properties, the twist direction has changed although the compressive behaviour of the bulk remains largely the same.

Table 5: Chain and bulk material coefficients for cases in parameter study where $n_2 = n_6$ and $n_3 = n_5$.

Case	n_2, n_6	n_3, n_5	Case	n_2, n_6	n_3, n_5
1	μ_0	$-1.5\mu_0$	6	$-0.25\mu_0$	$-0.25\mu_0$
2	$0.75\mu_0$	$-1.25\mu_0$	7	$-0.5\mu_0$	0
3	$0.5\mu_0$	$-\mu_0$	8	$-0.75\mu_0$	$0.25\mu_0$
4	$0.25\mu_0$	$-0.75\mu_0$	9	$-\mu_0$	$0.5\mu_0$
5	0	$-0.5\mu_0$			

Although not presented here, using the parameters given in table 4 but mechanically strong chains (e.g. with $\frac{n_4}{\mu_e} = 100$) leads to material having both angular and axial

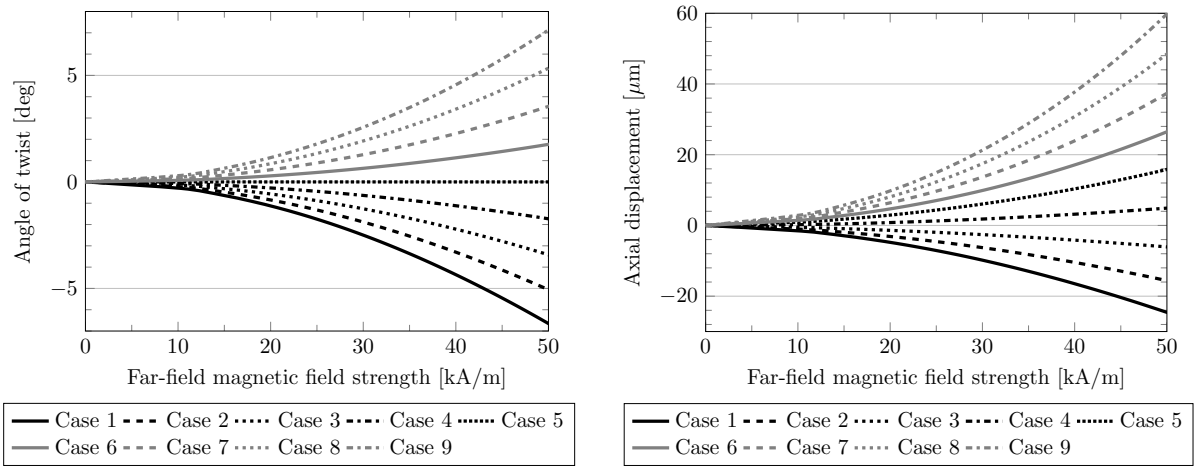

(a) Angle of twist

(b) Axial displacement

Figure 25: Influence of material coefficients on deformation at measurement point **P** when the chains are mechanically weak ($\frac{n_4}{\mu_e} = \frac{1}{10000}$). The material coefficients for each case are listed in table 5.

deformation characteristics similar to those shown in figure 25.

8 Conclusions and discussion

Dispersion of the particle-chains in magneto-active polymers is an undesirable but prevalent phenomenon as shown by several experiments, such as the ones presented in figure 1. Thus, it needs to be appropriately accounted for while constructing material models for these functional elastomers. In this paper, we have presented a procedure to model the effects due to dispersion of iron-particle chains in magneto-active elastomers. Based on similar developments in biomechanics, a probability-based structure tensor $\mathbf{G}$ that accounts for imperfect distribution of chains is defined and is used as an input to the energy density function. This is based on a parameter $\kappa \in [0, 1/3]$ that defines the degree of anisotropy. Additionally, as a simplification, we decompose the energies of the matrix and the chain phases – the latter based on the definition of a 'chain deformation gradient' $\mathbf{F}^c$ and a 'chain magnetic field' $\mathbb{H}^c$.

As is seen from the parametric studies in sections 6 and 7, the proposed model is able to capture the dependence of material response on the degree of anisotropy parameter κ. As $\kappa \to 0$, one obtains a perfectly anisotropic material and leads to stiffening of the material in the anisotropy direction. On the other hand, as $\kappa \to 1/3$, the material tends to become isotropic and the response of the chain phase and the matrix phase tend to align. Moreover, as is exemplified in figure 22, even for the case of perfect chain formation, one can obtain completely different magnetoelastic responses from the same geometry by making the chains stiffer or weaker than the bulk matrix. It has been extensively demonstrated that very different behaviours can be elicited from a material by appropriately modifying the constitutive model parameters.

A future course of research will be to employ image processing techniques to extract 3-D chain distribution parameters from the X-ray CT scans. This data will then be used

to provide numerical values to the structure tensor at every mesh point and appropriately model the material. Furthermore, using the models of rate-dependence and the experimental data on testing with magnetoelastic loading, a future aim is to provide physically and mathematically consistent material models for these smart polymers.

Acknowledgements

The support of this work by the European Research Council (ERC) through the Advanced Grant MOCOPOLY is gratefully acknowledged by the authors. The authors also thank Mr. Bastian Walter for MRE sample preparation and providing the images shown in figure 1.

References

[1] W. Bangerth, R. Hartmann, and G. Kanschat. deal.II – a general purpose object oriented finite element library. *ACM Trans. Math. Softw.*, 33(4):24/1–24/27, 2007.

[2] W. Bangerth, T. Heister, L. Heltai, G. Kanschat, M. Kronbichler, M. Maier, B. Turcksin, and T. D. Young. The `deal.ii` library, version 8.0. *arXiv preprint* *`http://arxiv.org/abs/1312.2266v3`*, 2013.

[3] A. Bermúdez, R. Rodríguez, and P. Salgado. A finite element method for the magnetostatic problem in terms of scalar potentials. *SIAM Journal on Numerical Analysis*, 46(3):1338–1363, 2008. doi: 10.1137/06067568X. URL `http://epubs.siam.org/doi/abs/10.1137/06067568X`.

[4] A. Boczkowska and S. F. Awietjan. Smart composites of urethane elastomers with carbonyl iron. *Journal of Materials Science*, 44(15):4104–4111, May 2009. ISSN 0022-2461. doi: 10.1007/s10853-009-3592-7.

[5] A. Boczkowska, L. Czechowski, M. Jaroniek, and T. Niezgoda. Analysis of magnetic field effect on ferromagnetic spheres embedded in elastomer pattern. *Journal of Theoretical and Applied Mechanics*, 48(3):659–676, 2010.

[6] H. Böse, R. Rabindranath, and J. Ehrlich. Soft magnetorheological elastomers as new actuators for valves. *Journal of Intelligent Material Systems and Structures*, 23 (9):989–994, 2012. doi: 10.1177/1045389X11433498.

[7] A. Bossavit. *Computational Electromagnetism. Variational Formulations, Complementarity, Edge Elements*, volume 2 of *Electromagnetism Series*. Academic Press, San Diego, 1 edition, 1998. ISBN-13: 978-0121187101.

[8] I. A. Brigadnov and A. Dorfmann. Mathematical modeling of magneto-sensitive elastomers. *International Journal of Solids and Structures*, 40(18):4659–4674, September 2003. ISSN 00207683. doi: 10.1016/S0020-7683(03)00265-8. URL `http://linkinghub.elsevier.com/retrieve/pii/S0020768303002658`.

[9] W. F. Brown. Magnetoelastic interactions. In C. Truesdell, editor, *Springer Tract in Natural Philosophy*. Springer-Verlag, Berlin Heidelberg New York, 1966.

[10] R. Bustamante. Transversely isotropic nonlinear magneto-active elastomers. *Acta Mechanica*, 210(3-4):183–214, July 2010. ISSN 0001-5970. doi: 10.1007/s00707-009-0193-0.

[11] R. Bustamante and R. Ogden. Nonlinear magnetoelastostatics: Energy functionals and their second variations. *Mathematics and Mechanics of Solids*, 18(7):760–772, 2012. doi: 10.1177/1081286512448347.

[12] R Bustamante and K R Rajagopal. On a new class of electroelastic bodies. I. *Proceedings of the Royal Society A*, 469(November 2012):20120521, 2013.

[13] R. Bustamante, A. Dorfmann, and R. W. Ogden. Numerical solution of finite geometry boundary-value problems in nonlinear magnetoelasticity. *International Journal of Solids and Structures*, 48(6):874–883, March 2011. ISSN 00207683. doi: 10.1016/j.ijsolstr.2010.11.021. URL `http://linkinghub.elsevier.com/retrieve/pii/S0020768310004208`.

[14] R. Bustamante, A. Dorfmann, and R.W. Ogden. Numerical solution of finite geometry boundary-value problems in nonlinear magnetoelasticity. *International Journal of Solids and Structures*, 48(6):874–883, 2011. ISSN 0020-7683. doi: http://dx.doi.org/10.1016/j.ijsolstr.2010.11.021. URL `http://www.sciencedirect.com/science/article/pii/S0020768310004208`.

[15] W. Chen, L. Sun, X. Li, and D. Wang. Numerical investigation on the magnetostrictive effect of magneto-sensitive elastomers based on a magneto-structural coupling algorithm. *Smart Materials and Structures*, 22(10): 105012–1–105012–15, 2013. doi: 10.1088/0964-1726/22/10/105012. URL `http://stacks.iop.org/0964-1726/22/i=10/a=105012`.

[16] K. Danas, S. V. Kankanala, and N. Triantafyllidis. Experiments and modeling of iron-particle-filled magnetorheological elastomers. *Journal of the Mechanics and Physics of Solids*, 60:120–138, 2012. doi: 10.1016/j.jmps.2011.09.006.

[17] T. A. Davis. Algorithm 832: Umfpack v4.3 – an unsymmetric-pattern multifrontal method. *ACM Transactions on Mathematical Software (TOMS)*, 30:196–199, 2004. doi: 10.1145/992200.992206.

[18] M. Destrade, B. Mac Donald, J. G. Murphy, and G. Saccomandi. At least three invariants are necessary to model the mechanical response of incompressible, transversely isotropic materials. *Computational Mechanics*, 52(4):959–969, April 2013. ISSN 0178-7675. doi: 10.1007/s00466-013-0857-4. URL `http://link.springer.com/10.1007/s00466-013-0857-4`.

[19] A. Dorfmann and R. W. Ogden. Nonlinear magnetoelastic deformations. *Quarterly Journal of Mechanics and Applied Mathematics*, 57(7):599–622, 2004.

[20] A. Dorfmann and R. W. Ogden. Some problems in nonlinear magnetoelasticity. *Journal of Applied Mathematics and Physics (ZAMP)*, 56(4):718–745, 2005.

[21] L. Dorfmann and R. W. Ogden. *Nonlinear Theory of Electroelastic and Magnetoelastic Interactions*. Springer, New York Heidelberg Dordrecht London, 2014.

[22] A. C. Eringen and G. A. Maugin. *Electrodynamics of Continua, Vol. 1*. Springer-Verlag, 1990.

[23] S. Federico and W. Herzog. On the anisotropy and inhomogeneity of permeability in articular cartilage. *Biomechanics and Modeling in Mechanobiology*, 7(5):367–78, October 2008. ISSN 1617-7940. doi: 10.1007/s10237-007-0091-0.

[24] E. Galipeau and P. Ponte Castãneda. The effect of particle shape and distribution on the macroscopic behavior of magnetoelastic composites. *International Journal of Solids and Structures*, 49(1):1–17, 2012. ISSN 0020-7683. doi: http://dx.doi.org/10.1016/j.ijsolstr.2011.08.014. URL `http://www.sciencedirect.com/science/article/pii/S0020768311003076`.

[25] T. C. Gasser, R. W. Ogden, and G. A. Holzapfel. Hyperelastic modelling of arterial layers with distributed collagen fibre orientations. *Journal of the Royal Society, Interface*, 3(6):15–35, February 2006. ISSN 1742-5689. doi: 10.1098/rsif.2005.0073.

[26] M.W. Gee, C.M. Siefert, J.J. Hu, R.S. Tuminaro, and M.G. Sala. ML 5.0 smoothed aggregation user's guide. Technical Report SAND2006-2649, Sandia National Laboratories, 2006.

[27] J. M. Ginder, S. M. Clark, W. F. Schlotter, and M. E. Nichols. Magnetostrictive phenomena in magnetorheological elastomers. *International Journal of Modern Physics B*, 16(17-18):2412–2418, 2002.

[28] M. A. Heroux. Aztecoo user's guide. Technical Report SAND2004-3796, Sandia National Laboratories, 2007.

[29] M. A. Heroux, R. A. Bartlett, V. E. Howle, R. J Hoekstra, J. J. Hu, T. G. Kolda, R. B. Lehoucq, K. R. Long, R. P. Pawlowski, E. T. Phipps, A. G. Salinger, H. K. Thornquist, R. S. Tuminaro, J. M. Willenbring, A. Williams, and K. S. Stanley. An overview of the Trilinos project. *ACM Transactions on Mathematical Software*, 31: 397–423, 2005. doi: 10.1145/1089014.1089021.

[30] G. A. Holzapfel. *Nonlinear solid mechanics*. John Wiley & Sons Ltd., West Sussex, England, 2007. ISBN 0 471 82304 X.

[31] G. A. Holzapfel and T. C. Gasser. A viscoelastic model for fiber-reinforced composites at finite strains : Continuum basis, computational aspects and applications. *Computational Methods in Applied Mechanics and Engineering*, 190:4379–4403, 2001.

[32] G. A. Holzapfel and R. W. Ogden. Constitutive modelling of arteries. *Proceedings of the Royal Society A*, 466(2118):1551–1597, March 2010. ISSN 1364-5021. doi: 10.1098/rspa.2010.0058.

[33] T. J. Hughes. *The Finite Element Method: Linear Static and Dynamic Finite Element Analysis*. Dover Publications Inc., New York, USA, 2000. ISBN 978-0486411811.

[34] H. Jasak and Ž Tuković. Automatic mesh motion for the unstructured finite volume method. *Transactions of Famena*, 30(2):1–20, 2006. URL http://www.scopus.com/inward/record.url?eid=2-s2.0-33847351298&partnerID=40&md5=1

[35] A.A. Johnson and T.E. Tezduyar. Mesh update strategies in parallel finite element computations of flow problems with moving boundaries and interfaces. *Computer Methods in Applied Mechanics and Engineering*, 119(1-2):73–94, 1994. URL http://www.scopus.com/inward/record.url?eid=2-s2.0-0028534257&partnerID=40&md5=f7

[36] M. R. Jolly, J. D. Carlson, and B. C. Muñoz. A model of the behaviour of magnetorheological materials. *Smart Materials and Structures*, 5(5):607–614, October 1996. ISSN 0964-1726. doi: 10.1088/0964-1726/5/5/009.

[37] S. V. Kankanala and N. Triantafyllidis. On finitely strained magnetorheological elastomers. *Journal of the Mechanics and Physics of Solids*, 52(12):2869–2908, December 2004. ISSN 00225096. doi: 10.1016/j.jmps.2004.04.007.

[38] K S Kannan and A Dasgupta. A nonlinear galerkin finite-element theory for modeling magnetostrictive smart structures. *Smart Materials and Structures*, 6(3):341, 1997. URL http://stacks.iop.org/0964-1726/6/i=3/a=011.

[39] Lance Ong-Siong Co Ting Keh, Jianfeng Zang, and Xuanhe Zhao. Magneto-rheological foams capable of tunable energy absorption. In *2013 Proceedings of IEEE Southeastcon*, pages 1–3. Ieee, April 2013. ISBN 978-1-4799-0053-4. doi: 10.1109/SECON.2013.6567490. URL http://ieeexplore.ieee.org/lpdocs/epic03/wrapper.htm?arnumber=6567490.

[40] S. Klinkel, C. Sansour, and W. Wagner. An anisotropic fibre-matrix material model at finite elastic-plastic strains. *Computational Mechanics*, 35(6):409–417, December 2004. ISSN 0178-7675. doi: 10.1007/s00466-004-0629-2.

[41] A. Kovetz. *Electromagnetic theory*. Oxford University Press, Oxford and New York, 2000.

[42] L. D. Landau and E. M. Lifshitz. *Electrodynamics of Continuous Media*. Pergamon Press, 1960.

[43] G. H. Livens. *The theory of electricity*. Cambridge University Press, 2 edition, 1962.

[44] H. V. Ly, F. Reitich, M. R. Jolly, and H. T. Banks. Simulations of particle dynamics in magnetorheological fluids. *Journal of Computational Physics*, 155(1):160–177, 1999. ISSN 0021-9991. doi: http://dx.doi.org/10.1006/jcph.1999.6335. URL http://www.sciencedirect.com/science/article/pii/S0021999199963350.

[45] B. Marvalova. *Modelling and Simulation*, chapter Modelling of Magnetosensitive Elastomers, pages 245–260. I-Tech Education and Publishing, 2008. ISBN: 978-3-902613-25-7.

[46] G. A. Maugin. *Continuum Mechanics of Electromagnetic Solids*. North-Holland, 1988.

[47] G. A. Maugin. On modelling electromagnetomechanical interactions in deformable solids. *International Journal of Advances in Engineering Sciences and Applied Mathematics*, 1:25–32, 2009.

[48] G. A. Maugin and A. C. Eringen. On the equations of the electrodynamics of deformable bodies of finite extent. *Journal de Mecanique*, 16(1):101–146, 1977.

[49] B. Nedjar. An anisotropic viscoelastic fibre-matrix model at finite strains: Continuum formulation and computational aspects. *Computer Methods in Applied Mechanics and Engineering*, 196(9-12):1745–1756, February 2007. ISSN 00457825. doi: 10.1016/j.cma.2006.09.009.

[50] M. Otténio, M. Destrade, and R. W. Ogden. Incremental magnetoelastic deformations, with application to surface instability. *Journal of Elasticity*, 90(1):19–42, 2008. doi: 10.1007/s10659-007-9120-6.

[51] Y. H. Pao and K. Hutter. Electrodynamics for moving elastic solids and viscous fluids. *Proceedings of the IEEE*, 63(7):1011–1021, 1975. ISSN 0018-9219. doi: 10.1109/PROC.1975.9878. URL `http://ieeexplore.ieee.org/lpdocs/epic03/wrapper.htm?arnumber=1451808`.

[52] S. Rudykh and K. Bertoldi. Stability of anisotropic magnetorheological elastomers in finite deformations: A micromechanical approach. *Journal of the Mechanics and Physics of Solids*, 61(4):949–967, 2013. ISSN 0022-5096. doi: http://dx.doi.org/10.1016/j.jmps.2012.12.008. URL `http://www.sciencedirect.com/science/article/pii/S0022509613000045`.

[53] E. Salas and R. Bustamante. Numerical solution of some boundary value problems in nonlinear magneto-elasticity. *Journal of Intelligent Material Systems and Structures*, 2014. doi: 10.1177/1045389X14522533. URL `http://jim.sagepub.com/content/early/2014/02/10/1045389X14522533.abstract`.

[54] C. Sansour. On the physical assumptions underlying the volumetric-isochoric split and the case of anisotropy. *European Journal of Mechanics - A/Solids*, 27(1):28–39, January 2008. ISSN 09977538. doi: 10.1016/j.euromechsol.2007.04.001.

[55] P. Saxena, M. Hossain, and P. Steinmann. A theory of finite deformation magneto-viscoelasticity. *International Journal of Solids and Structures*, 50(24):3886–3897, 2013. doi: 10.1016/j.ijsolstr.2013.07.024.

[56] P. Saxena, M. Hossain, and P. Steinmann. Nonlinear magneto-viscoelasticity of transversally isotropic magneto-active polymers. *Proceedings of the Royal Society A*, 470:20140082, 2014.

[57] Mark D. Semon and John R. Taylor. Thoughts on the magnetic vector potential. *American Journal of Physics*, 64(11):1361–1369, 1996. doi: 10.1119/1.18400. URL `http://scitation.aip.org/content/aapt/journal/ajp/64/11/10.1119/1.18400`.

[58] M. Shams, M. Destrade, and R. W. Ogden. Initial stresses in elastic solids : Constitutive laws and acoustoelasticity. *Wave Motion*, 48(7):552–567, 2011. ISSN 0165-2125. doi: 10.1016/j.wavemoti.2011.04.004. URL http://dx.doi.org/10.1016/j.wavemoti.2011.04.004.

[59] J. C. Simo, R. L. Taylor, and K. S. Pister. Variational and projection methods for the volume constraint in finite deformation elasto-plasticity. *Computer Methods in Applied Mechanics and Engineering*, 51:177–208, 1985. doi: 10.1016/0045-7825(85)90033-7.

[60] T. M. Simon, F. Reitich, M. R. Jolly, K. Ito, and H. T. Banks. The effective magnetic properties of magnetorheological fluids. *Mathematical and Computer Modelling*, 33(1–3):273–284, 2001. ISSN 0895-7177. doi: http://dx.doi.org/10.1016/S0895-7177(00)00244-2. URL http://www.sciencedirect.com/science/article/pii/S0895717700002442. Computation and control {VI} proceedings of the sixth Bozeman conference.

[61] A. J. M. Spencer. Theory of invariants. In A. C. Eringen, editor, *Continuum Physics, Vol. I*, pages 239–353. Academic, New York, 1971.

[62] D. J. Steigmann. On the Formulation of Balance Laws for Electromagnetic Continua. *Mathematics and Mechanics of Solids*, 14(4):390–402, September 2009. ISSN 1081-2865. doi: 10.1177/1081286507080808. URL http://mms.sagepub.com/cgi/doi/10.1177/1081286507080808.

[63] P. Steinmann. *Mechanics and Electrodynamics of Magneto- and Electro-elastic Materials*, chapter Computational Nonlinear Electro-Elasticity – Getting Started. Springer Vienna, 2011. doi: 10.1007/978-3-7091-0701-0_5.

[64] H. F. Tiersten. Coupled magnetomechanical equations for magnetically saturated insulators. *Journal of Mathematical Physics*, 5(9):1298–1318, 1964.

[65] Z. Varga, G. Filipcsei, and M. Zrínyi. Smart composites with controlled anisotropy. *Polymer*, 46:7779–7787, 2005. doi: 10.1016/j.polymer.2005.03.102.

[66] Z. Varga, G. Filipcsei, and M. Zrinyi. Magnetic field sensitive functional elastomers with tuneable elastic modulus. *Polymer*, 47(1):227–233, January 2006. ISSN 00323861. doi: 10.1016/j.polymer.2005.10.139.

[67] F. Vogel, R. Bustamante, and P. Steinmann. On some mixed variational principles in magneto-elastostatics. *International Journal of Non-Linear Mechanics*, 51(0):157 – 169, 2013. ISSN 0020-7462. doi: http://dx.doi.org/10.1016/j.ijnonlinmec.2012.12.005. URL http://www.sciencedirect.com/science/article/pii/S0020746212001989.

[68] F. Vogel, J-P. Pelteret, S. Kässmair, and P. Steinmann. Magnetic force and torque on particles subject to a magnetic field. *European Journal of Mechanics A/Solids*, 2014. Accepted.

[69] D. K. Vu, P. Steinmann, and G. Possart. Numerical modelling of non-linear electroelasticity. *International Journal for Numerical Methods in Engineering*, 70:685–704, 2007. doi: 10.1002/nme.1902.

[70] M. Yalcintas and H. Dai. Vibration suppression capabilities of magnetorheological materials based adaptive structures. *Smart Materials and Structures*, 13(1):1–11, 2004.

[71] Y.M. Yin, L.Z. Sun, and J.S. Chen. Magneto-elastic modeling of composites containing chain-structured magnetostrictive particles. *Journal of the Mechanics and Physics of Solids*, 54(5):975–1003, 2006. ISSN 0022-5096. doi: http://dx.doi.org/10.1016/j.jmps.2005.11.007. URL `http://www.sciencedirect.com/science/article/pii/S002250960500222X`.

[72] Q.-S. Zheng. Theory of representations for tensor functions - A unified invariant approach to constitutive equations. *Applied Mechanics Review*, 47(11):545–587, 1994.

[73] X-J. Zheng and X. Wang. Analysis of magnetoelastic interaction of rectangular ferromagnetic plates with nonlinear magnetization. *International Journal of Solids and Structures*, 38(48–49):8641–8652, 2001. ISSN 0020-7683. doi: http://dx.doi.org/10.1016/S0020-7683(01)00100-7. URL `http://www.sciencedirect.com/science/article/pii/S0020768301001007`.